Linear Impact of Bicycle Helmet – Experimental Testing and FE-modelling

KTH Thesis Report

Ludvig Dahlin
Ebba Larsson Regnström

KTH ROYAL INSTITUTE OF TECHNOLOGY

THE SCHOOL OF ENGINEERING SCIENCES

Authors

Ludvig Dahlin <ludvigd@kth.se> and Ebba Larsson Regnström <ebbalr@kth.se>
School of Engineering Sciences
KTH Royal Institute of Technology

Place for Project

Stockholm, Sweden

Examiner

Jonas Neumeister
KTH Royal Institute of Technology

Supervisor

Johan Weman

POC Sports

Abstract

The aim with this master thesis was to set up a FE-simulation of an impact test of a bike helmet in LS-DYNA that correlates well with the peak acceleration score of a real life impact test. Furthermore, a parametric study has been performed in LS DYNA to investigate the robustness of the model, as well as to see which parameters have a great influence on the peak acceleration score. To investigate the acceleration of the helmet, helmet drop tests have been performed at the Borås RISE lab. Building an FE-model of the helmet drop test required multiple iterations to ensure stability and accuracy of the model. The steps of the modelling process included investigating previous simulations of helmet impacts in LS-DYNA, preprocessing of CAD, defining material models and establishing contact and boundary conditions. The parameters that have proven to have a great impact on the peak acceleration value are the tensile stress cutoff, the PC shell thickness, the strain rate dependency, and the EPS thickness. A conclusion of this work is that FE modelling is a way to approximate the peak acceleration value for linear impact tests, and a useful tool for investigating design parameters. The density of the EPS foam is shown to have a large influence on the peak acceleration value in both the experimental tests and the FE simulation. From the FE simulationns, the thickness of the EPS, as well as the thickness of the PC shell have shown to have a great impact on the peak acceleration score.

Acknowledgements

We are grateful to POC Sports for the opportunity of doing this master thesis. We want to thank our company supervisor Johan Weman, as well as Nicolò Dall'Acqua for their input and support during this thesis. We would also like to thank our examiner Jonas Neumeister for the valuable discussions we had, and for guiding us through this work.

Acronyms

CAD   Computer Aided Design

EPS   Expanded Polystyrene

FEA   Finite Element Analysis

FEM   Finite Element Method

PC   Polycarbonate

Contents

Chapter 1

Introduction

Using a bicycle helmet is an effective way of reducing the risk of brain injuries in the event of a crash [1]. There are regulations to ensure the security of a bicycle helmet, and since the brain is sensitive to high accelerations, the standards are usually based on the peak acceleration score from a drop test [2]. A bicycle helmet commonly consists of a foam liner, and an outer shell made from polycarbonate. The helmet deforms elastically and plastically to absorb the impact energy and distribute the resultant forces from the crash, to prevent large accelerations of the head [3].

Many cyclists, especially on a professional level, look for a light weight helmet, with low aerodynamic drag and good ventilation [4]. To design a bicycle helmet that meets the criteria of the customer, but at the same time fulfils the safety standards, several design iterations can be needed. A finite element simulation of the experimental setup of a helmet verification test would reduce both the time and the cost of the product development process, and lead to more protective, and faster helmets.

1.1 Purpose

The purpose of this work is to complement real life drop tests of bicycle helmets with FE simulations, and thus reduce the time and costs of helmet production from idea to final product. With a simulation, many different designs could be investigated before the production, and the helmet could be better designed to prevent head injuries.

1.2 Goal

The goal with this master thesis is to set up a FE-simulation of an impact test of a bike helmet in LS-DYNA that correlates well with the peak acceleration score of a real life impact test. Furthermore, a parametric study will be performed in LS DYNA to investigate the robustness of the model, as well to see which parameters have a great influence on the peak acceleration score.

Chapter 2

Background

Nowadays almost all bicycle helmets consist of an Expanded Polystyrene (EPS) foam liner, with an outer shell of Polycarbonate (PC). While the PC distributes the load and absorbs some energy through shell deformation and buckling, the EPS dissipates the majority of the energy (70-90 %) from the impact through a visco-plastic process [5] [6] [7]. The helmet used in this master thesis is the Ventral Air MIPS helmet from POC Sports, pictured in Figure 2.0.1. The Ventral Air helmet is specifically designed for road biking, with an aerodynamic profile and a light weight design [8]. To keep the weight low, it is preferable to use a low-density EPS liner, however the energy absorbing properties change with the density of the EPS [9]. This master thesis will investigate three different EPS densities in a finite element analysis (FEA), and then compare the results with experimental tests.

Figure 2.0.1: Ventral Air MIPS helmet, from POC. [10]

.

2.1 Expanded polystyrene foam

The behaviour of EPS in compression can commonly be divided into three different zones, as can be seen in the compressive stress-strain curve for the foam, see Figure 2.1.1. The first zone is the linear elastic part of the curve, characterised by the linear relation between the stress and strain. At this point the cell walls of the EPS foam are bending. When the yield point for the material is reached, the stress-strain curve transitions into the second zone. The second zone is characterised by a near horizontal stress plateau due to buckling of the cellular struts, resulting in plastic collapse of the foam. This material behaviour is desired since it is responsible for most of the energy dissipation during the deformation process, however it also entails nonrecoverable deformations [11]. Lastly, in the third zone, at large strains, densification occurs from the cells in the foam having completely collapsed or the cell walls having ruptured from the increased gas pressure within the foam. The collapsed cells start to compress against one another leading to an increase of density, which results in a steep stress-strain curve [12] [11] [6].
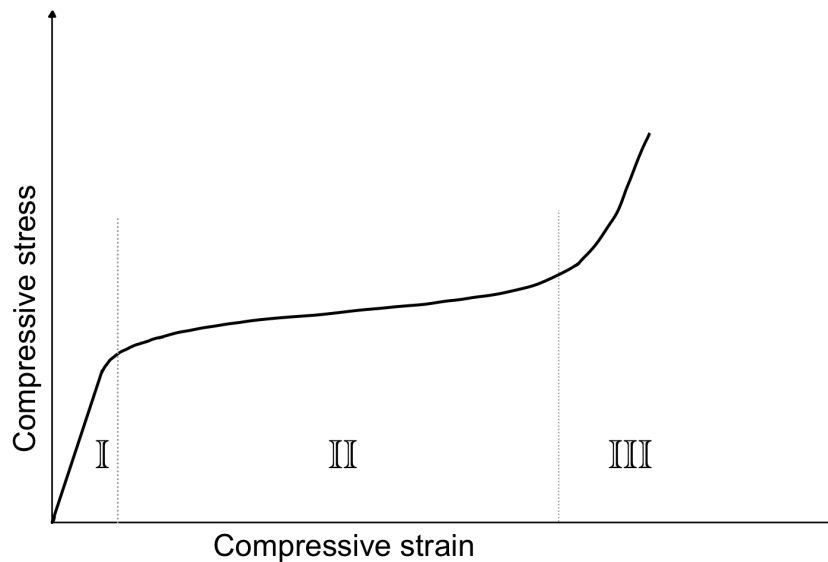

Figure 2.1.1: Stress-strain behaviour of EPS foams in compression with the three different zones illustrated.

During compression EPS shows a strain-rate dependent behaviour with the stress-strain curve changing depending on the strain-rate. The shear stress of EPS is also

both strain-rate and density dependent [13].

The mechanical properties of EPS change with temperature and humidity. When exposed to cold temperatures, the EPS foam hardens, resulting in a higher stiffness of the material. On the contrary, when heated up, the material becomes softer [6]. When exposed to cyclic temperature changes, both the elastic and shear modulii of the material are at risk of reduction [14]. When developing bicycle helmets, it is of high importance to use EPS that works well under a variety of conditions.

2.1.1 Foam density

The density of the EPS foam plays an important role for how the helmet will behave during impact. The Young's modulus will increase with the density, resulting in a stiffer material with a higher yield stress, see Figure 2.1.2. the yield stress is the stress at which the crushing of the foam begins. This relation between the density and stiffness has a direct impact on the energy absorption capabilities of the foam, with a higher density foam being able to absorb more energy during impact. However, due to the increased stiffness, a higher density foam will also transfer higher loads to the head [11]. On the other hand, with a lower density the risk of bottoming out during high loads increase. If the EPS in a helmet bottoms out during impact the head will experience an abrupt increase of resultant acceleration.

When designing a bicycle helmet it is of high importance to choose the right foam density, as well as a good foam thickness. For bicycle helmets it is common to use densities between 20 and 100gpl, and thicknesses varying from 30 to 40 mm [15]. For this master thesis we have obtained uni axial, compressive stress-strain curves from POC for EPS foams with three different densities: 60gpl, 80gpl and 100gpl. The stress-strain curves can be seen in Figure 2.1.2.
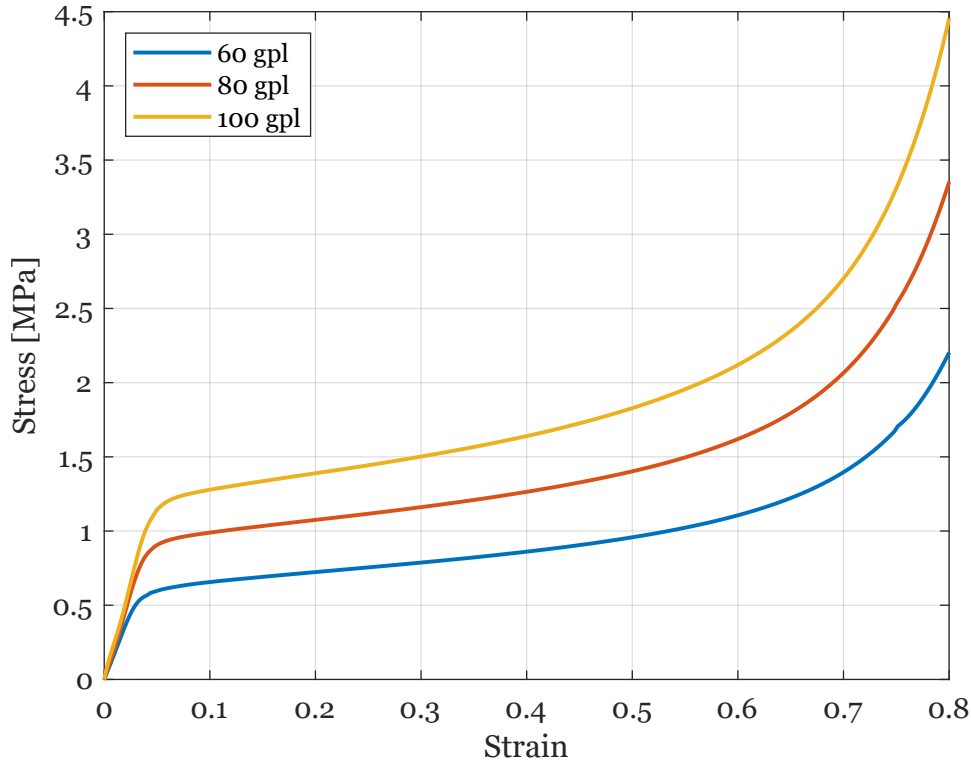
Figure 2.1.2: Compressive stress-strain curves for three different densities of EPS.

2.2 Finite element method

The finite element method (FEM) is a numerical method for solving complex mechanical problems by dividing the geometry into many small, finite, elements. For this project we have chosen to use LS-DYNA to make the FE simulation. LS-DYNA is a multiphysics software that specializes in dynamical problems and impact simulations. In this master thesis, LS-PrePost is used as the pre- and post processor, and LS-Run is the solver. LS-DYNA solves static problems implicitly, and dynamic problems either implicitly or explicitly.

In explicit analysis, external and internal forces are added in every node. By multiplying the nodal force vector with the inverted diagonal mass matrix, the nodal acceleration, d, is obtained. By integrating the nodal acceleration over time at state n, the velocity, v, is found at state $n + \frac{1}{2}$, allowing the calculation of the displacement, d, at state $n + 1$. From this, one can obtain the strain and the stress. Thereafter, the cycle is repeated for the next time step. The explicit analysis relies on the accelerations, velocities, and displacements at time n, as seen in equation 2.1.

$$d^{n+1} = f(a^n, d^n, v^n, d^{n-1}, ...)$$ (2.1)

As everything is known for the explicit time integration, the equation can be solved without iterations. The implicit analysis, on the other hand, works iteratively by inverting the global stiffness matrix, then computing the displacement by trying to find the equilibrium of the system at state $n + 1$. To solve the implicit analysis, information is needed about the acceleration and velocity at time $n + 1$, see equation 2.2.

$$d^{n+1} = f(a^{n+1}, d^{n+1}, d^n, v^n, ...)$$ (2.2)

For the implicit analysis, the user can choose the time step freely, whilst for the explicit analysis, the time step is governed by the Courant time step. The Courant time step is determined by the time it takes for a sound wave to to pass an element. The implicit analysis is more time consuming and computationally heavy, and thus more costly, especially for large systems [16].

2.3 Test Standard

The European standard, considering helmets for pedal cyclists and for users of skateboards and roller skates, is the EN 1078:2012+A1:2012 standard. It specifies construction requirements for the helmet, experimental setup for the test and limits for the peak acceleration. The helmet should have a low weight, allow for ventilation of the head, be easy to put on and remove, allow for the use of spectacles, and not considerably reduce the ability of the wearer to hear traffic noise [17]. The helmet's ability to protect should still be satisfactory when subjected to different climatic conditions. This is tested by exposing the helmet to high and low temperatures, and additionally artificial ageing by exposure to ultraviolet irradiation and water [17][18].

For the impact tests the headforms used should fall within the EN 960:2006 standard. The helmet is supported by the headform in a guided free fall onto the anvil, resulting in the impact force being applied dynamically. When performing an impact test on a flat anvil the impact velocity should be 5.42-5.52 m/s and the resulting peak acceleration experienced by the headform should not exceed 250 g. The flat anvil should be circular with a diameter of 130 mm. [17].

Chapter 3

Experiment

To investigate the peak acceleration of the bike helmet, according to the EN 1078 standard, helmet drop tests were performed at RISE Research Institutes of Sweden in Borås. Linear impact tests were performed for two different impact points, crown and back, as shown in Figure 3.0.1. The impact surface used was a flat, circular, steel anvil with a diameter of 130 mm.
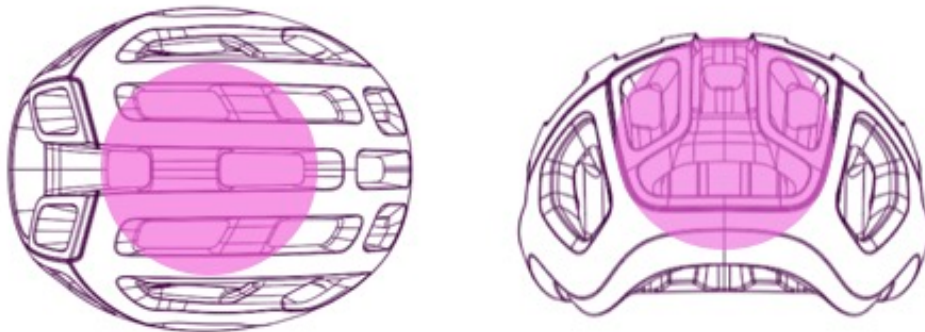

Figure 3.0.1: The impact points for crown (left) and back (right).

The drop height was calibrated for the desired velocity using an already crashed helmet. The helmet was placed on a 575 J EN960 headform, with the straps closed, and then positioned in a guided free fall drop tower, shown in Figure 3.0.2. The head form had a weight of 4.7 ± 0.13 kg. Two bungee straps were used to secure the helmet, to keep it from bouncing off during impact. The helmet was then lifted to the calibrated height, and dropped onto the flat anvil. The data from the accelerometer of the head form was extracted, and the resultant acceleration was plotted against the time.
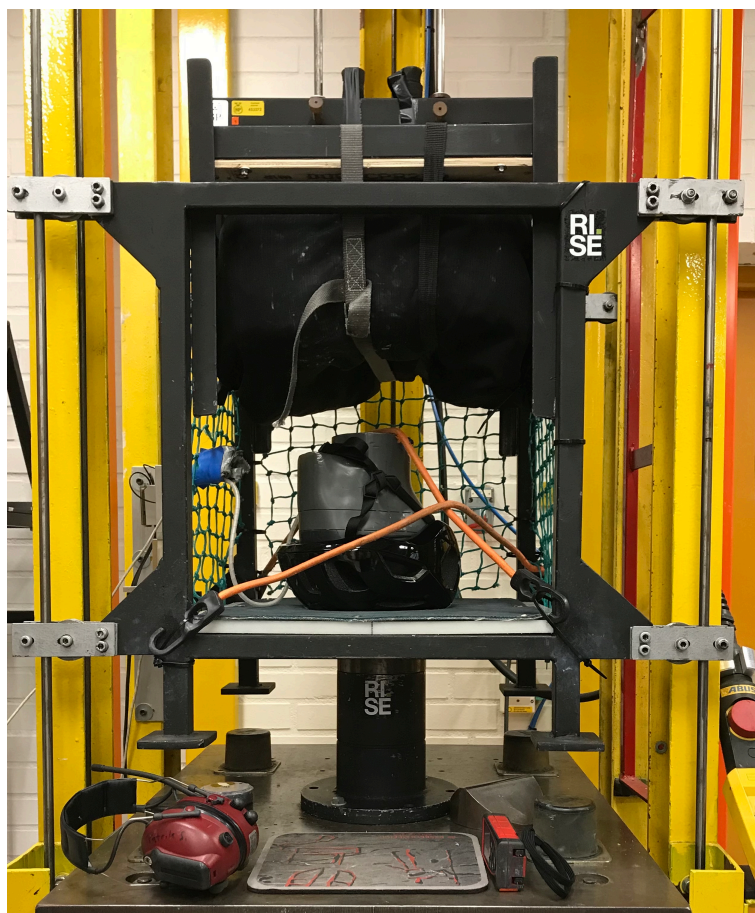
Figure 3.0.2: Drop tower set up for crown impact.

The experiment was repeated for two cases (back and crown impact), three densities of the EPS foam and three impact velocities, as seen in Table 3.0.1. For the tests at the highest velocity, the helmets had been crashed once before at a different impact point, which is acceptable in accordance with the standards.

Table 3.0.1: Number of tests for crown and back impact for the different velocities and densities.

Number of tests for crown impact				Number of tests for back impact		
Velocity / Density	60 gpl	80 gpl	100 gpl	60 gpl	80 gpl	100 gpl
5.42 m/s	3	3	3	3	3	3
6.5 m/s	3	3	3	0	0	0
7.7 m/s	1*	1*	1*	1*	1*	1*
*The helmets had been crashed once before at a different impact point						

The acceleration vs time plots of the crown impact at 5.42 m/s for the helmets with a density of 60 gpl are shown in Figure 3.0.3. All the tests show similar curves, however the peak acceleration value varies 1.5-5.5 % among the tests. Around the value of 2.5 ms on the x-axis, one can discern a load dip for all the curves.
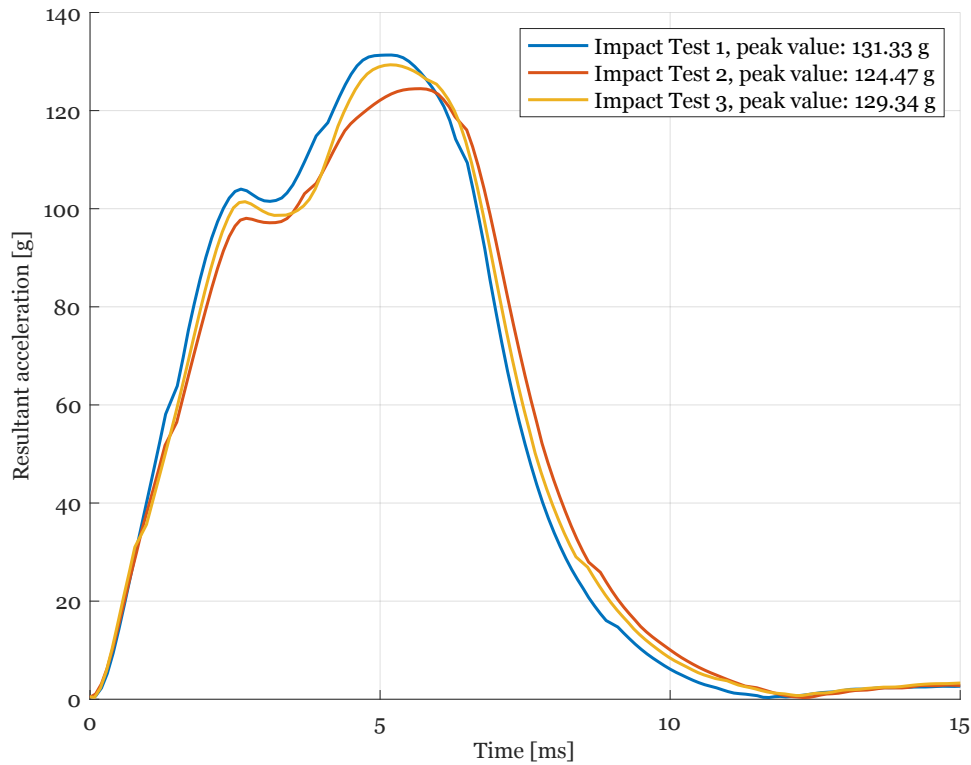

Figure 3.0.3: Acceleration vs time plots for the three tests of 60 gpl density crown impact at 5.42 m/s.

For the back impact tests of the 60 gpl density at 5.42 m/s, all the tests follow a similar curve, as seen in Figure 3.0.4. The peak acceleration value varies 2.2-4.9 % among the tests.
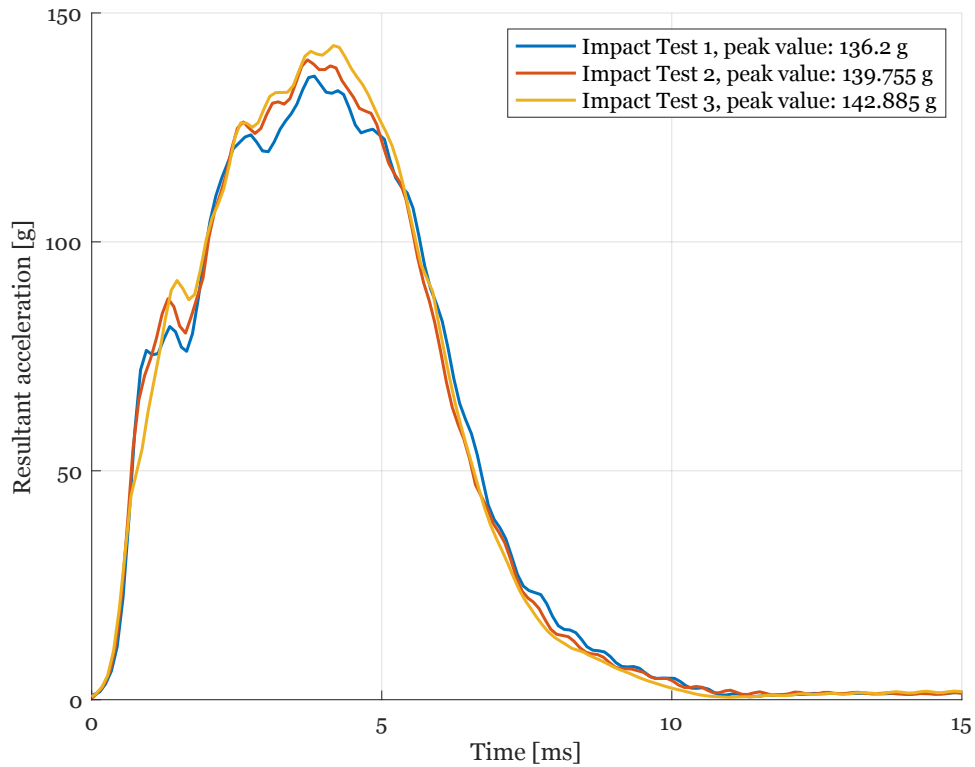
Figure 3.0.4: Acceleration vs time plots for the three tests of 60 gpl density back impact at 5.42 m/s.

Figure 3.0.5 shows the average curves of the three crown impact tests for each density at 5.42 m/s. It can be seen that the initial steepness of the curve increases with the density of the helmets, as well as the peak acceleration. The impact time, however, decreases with the increase in density. For all the densities, a load dip occurs at approximately 3 ms.
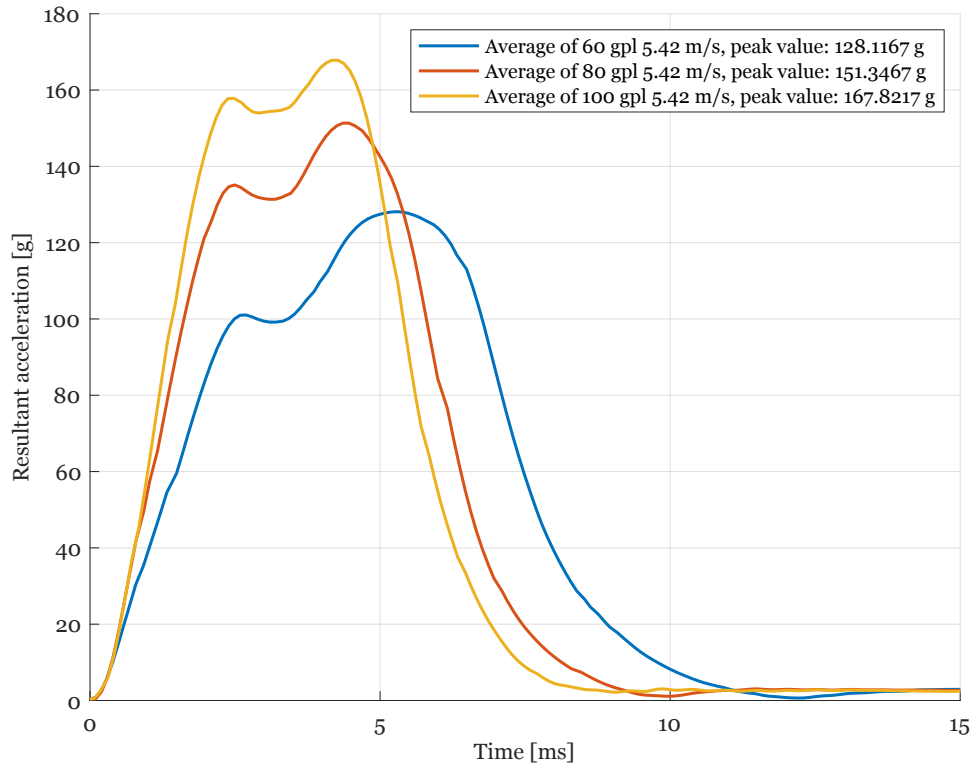
Figure 3.0.5: Acceleration vs time plots for the average plots of 60 gpl, 80 gpl and 100 gpl for crown impact at 5.42 m/s.

To see how the helmets respond to different velocities, the average of the tests for 60 gpl crown impact have been plotted for the three velocities in Figure 3.0.6. The impact time does not vary with the velocity, but the peak acceleration increases. For 5.42 m/s and 6.5 m/s, the plots follow a similar shape, whereas the 7.7 m/s shows a pointier shape with less of a load dip at 3 ms. It is worth mentioning that the helmet tested at 7.7 m/s was crashed once before, as well as that only one test was done for this case and thus the plot for 7.7 m/s is not an average of 3 tests, as is the case for 5.42 m/s and 6.5 m/s.
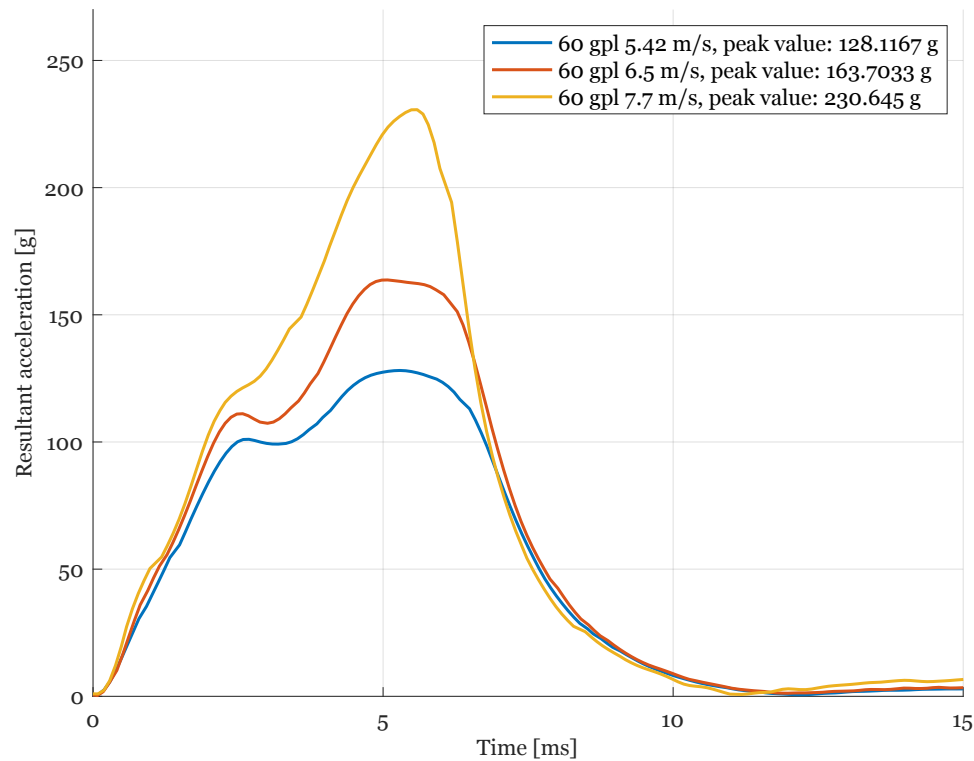
Figure 3.0.6: Acceleration vs time plots of 60 gpl for crown impact at 5.42, 6.5 and 7.7 m/s.

Figure 3.0.7 shows the back impact tests for all the densities at the velocity of 5.42 m/s. The peak acceleration increases with the density, as the impact time decreases. There seems to be a load retardation at 2 ms, however it is not very noticable for the density of 80 gpl.
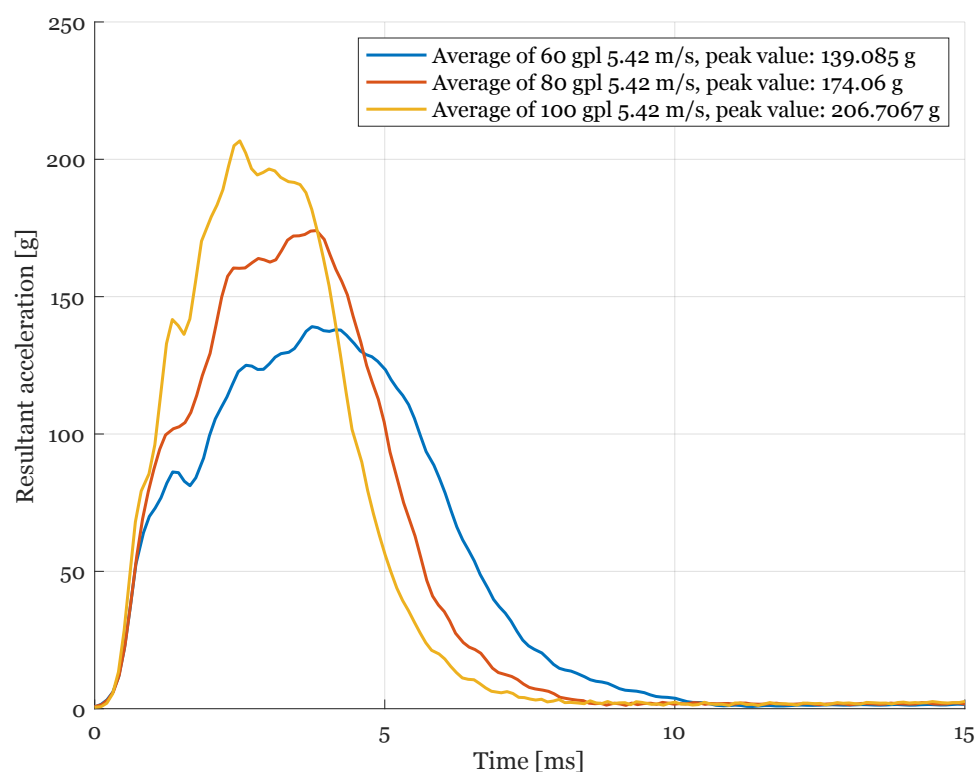
Figure 3.0.7: Acceleration vs time plots of 60, 80 and 100 gpl at back impact at 5.42 m/s.

The back impact for the 60 gpl helmet is plotted for the two different velocities in Figure 3.0.8, where once again, a load dip is discerned at around 2 ms. The peak acceleration is remarkably higher for the 7.7 m/s case, compared to that of 5.42 m/s.
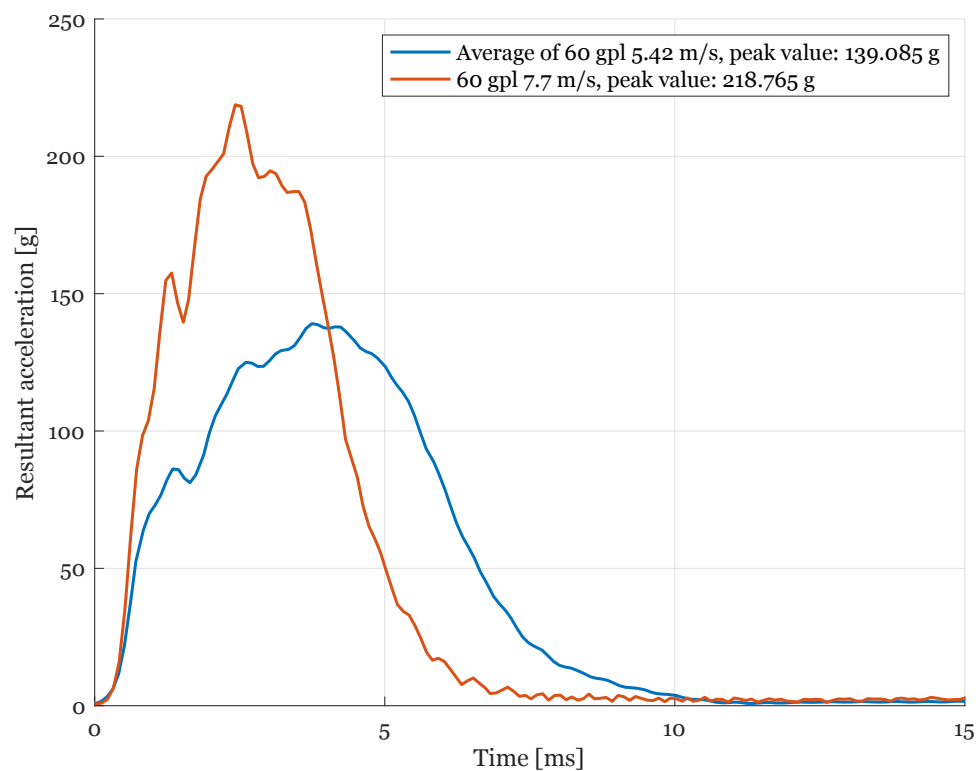
Figure 3.0.8: Acceleration vs time plots for 60 gpl back impact at 5.42 m/s and 7.7 m/s.

Chapter 4

FE-model

Building a FE-model of the helmet drop test required multiple iterations of each step of the modelling process to ensure stability and accuracy of the model. The steps of the modelling process include investigating previous simulations of helmet impacts in LS-DYNA, preprocessing of CAD models, defining material models and establishing contact conditions and boundary conditions. Each modelling step is described in further detail in this chapter.

4.1 Preprocessing of CAD models

The CAD model for the Ventral Air helmet was provided by POC. The initial model included the EPS foam liner, PC shell, strap anchors, size adjustment system, comfort liner and rotational impact protection system. The model of the helmet can be seen in Figure 4.1.1.
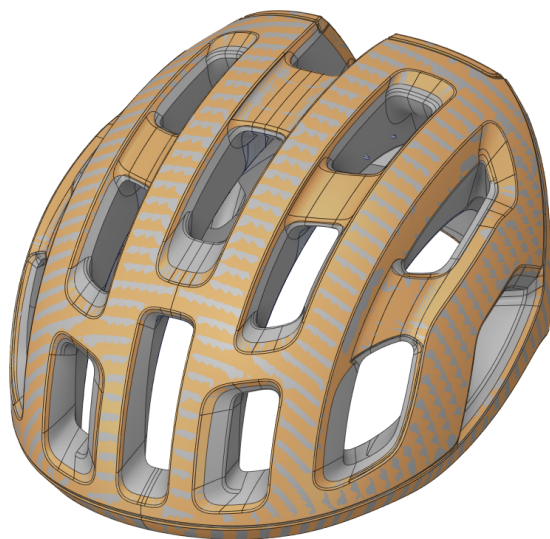
Figure 4.1.1: POC Ventral Air.

The EN960 headform was also provided by POC, see Figure 4.1.2. The meshing of the geometries in the FE model were done in Altair HyperMesh Student Edition.
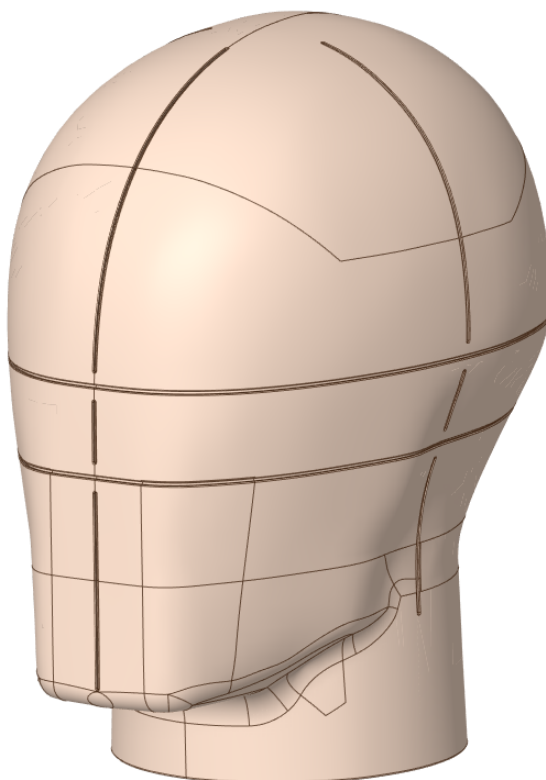

Figure 4.1.2: CAD model of EN960 headform.

Since all the impacts that were investigated occur in the helmet's sagittal plane, only

one half of the helmet and head was modelled with a symmetry boundary conditions, see Figure 4.1.3.
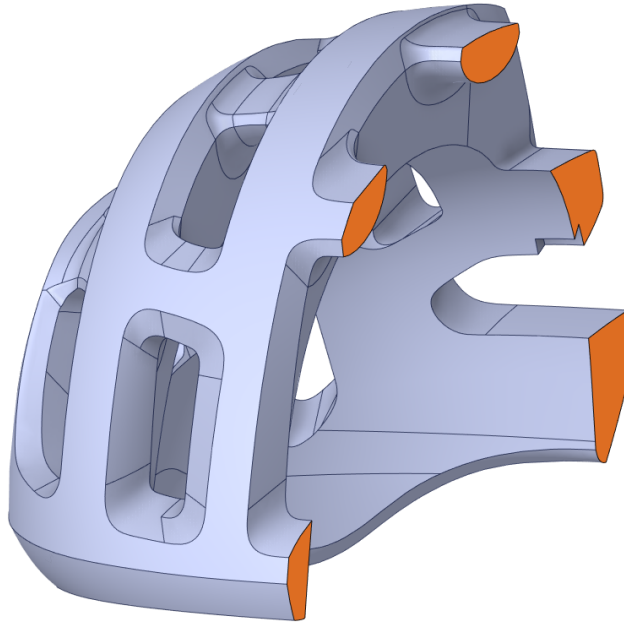

Figure 4.1.3: Half of POC Ventral Air.

4.1.1 Clean up of CAD models

The CAD models were cleaned up to ease the process of meshing. The cleaning was performed by altering the initial geometry through removing fine and small details. The EPS lining and PC shell were subjected to the most change and where modified by removing small fillets, merging surfaces, filling small holes and gaps. The strap anchors and size adjustment system and the rotational impact protection system were also removed since it was deemed that they would greatly increase the complexity of the model without having any substantial contribution to the linear impact results. Furthermore, the comfort liner was neglected in the model as it was considered to have an insignificant influence on the peak acceleration of the simulation. The *autocleanup* tool in HyperMesh was also used to suppress small or overlapping edges to allow for a better flow in the mesh.

4.1.2 Meshing

The meshing of the helmet parts and headform was mainly performed in Altair HyperMesh with only the mesh for the anvil being built in LS-PrePost.

Foam / EPS

The EPS liner was meshed with 113000 solid tetrahedral elements. The mesh was generated by first using a 2D-surface mesh consisting of R-trias elements with a target element size of 3 mm. The number of elements at critical regions were increased to improve accuracy of the model. The critical regions were defined as areas of the geometry that were suspected to be subjected to large deformations. The solid elements were then obtained from 3D tetra meshing using the 2D-surface mesh as base and splitting quad elements into trias. Lastly, the 2D-surface mesh was removed.

Shell / PC

The PC shell was scaled up with 1% to remove most of the initial penetration between the EPS and PC. By using the automesh tool, a mesh was generated, consisting of 13009 2D-surface quadrilateral elements with a target element size of 1.5mm.

Headform

For the EN960 Headform, a volume tetra mesh with surface elements and 3D elements was used. The surface elements were R-trias and the 3D elements were tetras. The target element size were 10mm, resulting in 16502 solid elements.

Anvil

The anvil was modelled as a circular shell with radius 65 mm and element density 80 using the Shape Mesher tool in LS-PrePost, resulting in a mesh with 1920 quadratic 2D elements.

4.2 Material models, element formulations, and contact definitions

To prepare the simulation, all the meshed components of the helmet were assembled in LS-DYNA. The material cards and contact conditions for the components were defined, as well as the initial and boundary conditions for the model.

4.2.1   Helmet shell

The outer shell of the POC ventral air is made of a thin layer polycarbonate (PC). To model the material behaviour for the PC, the MAT_ELASTIC keyword was used with the material data taken from literature, see Table 4.2.1 [3] [19]. The MAT_ELASTIC keyword is a hypoelastic material model.

To model the PC, shell elements with a thickness of 0.7 mm were used. The shell elements uses the element formulation ELEFORM=16: Fully integrated shell element (very fast). The shell element 16 helps with preventing locking of elements and is well suited for problems with in-plane bending [20].

The simplification of disregarding the plastic behaviour of the PC was a conscious choice since obtaining relevant material data proved to be difficult. This choice then arguably results in a stiffer material model compared to the one seen in reality.

Table 4.2.1: Material properties for PC shell.

PC shell	
Density [kg/m^3]	1200
Young's modulus [GPa]	2.2
Poisson's ratio	0.37

4.2.2   EPS foam

The EPS liner was modelled with solid elements and the material properties for the foams with different densities were provided by POC, see Table 4.2.2. Since large strains were expected to occur in the EPS during the impact the element formulation ELEFORM=13: 1 point nodal pressure tetrahedron for bulk forming, was chosen since it is well suited for tetrahedral elements and problem with large strains [21].

Table 4.2.2: Material properties for EPS foam.

EPS Foam	1	2	3
Density [g/mm^3]	60	80	100
Young's modulus [GPa]	0.0181	0.0213	0.0331
Poisson's ratio	0	0	0

For the material keyword, MAT_CRUSHABLE_FOAM was used to capture the

behaviour of the EPS during compression. The keyword requires uni-axial yield stress-strain curves as input [22] and these curves were also provided by POC. However, it was necessary to modify the load curves since the solvers time step calculation include the final slope of the curve and due to densification towards the end, it resulted in extreme run times or errors occurring in the solver. The curves where modified by excluding values after 0.9 strain and curve fitting a third degree polynomial to the values on the strain value interval 0.75 to 0.9. The functions obtained from the curve fitting were then used to extrapolate the curves from the point of exclusion. The modified curves can then be seen in Figure 4.2.1.
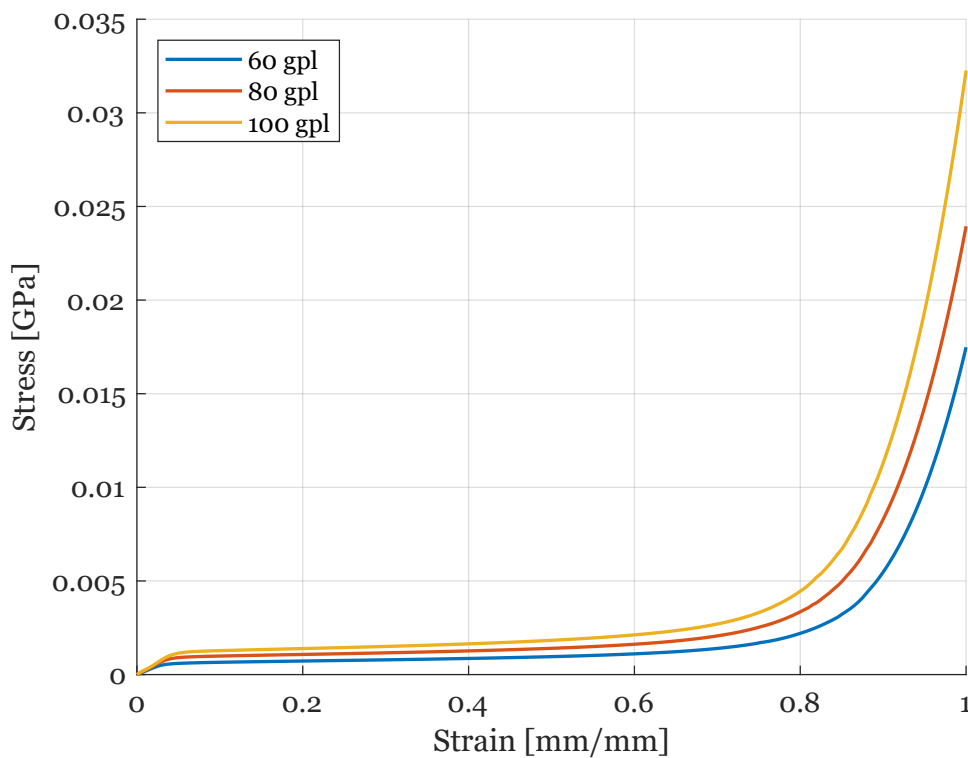
Figure 4.2.1: Modified EPS stress-strain curves.

The crushable foam keyword results in an isotropic material model with fully elastic unloading. Tension is accounted for through a tensile cutoff term, named TSC. The tension is elastic until it reaches the TSC value, then it becomes perfectly plastic. The material model does not take strain rate effects into account, such as viscoplastic effects, other than by an optional damping parameter called DAMP [20][22]. The parameter of TSC was set to 0.0001 GPa, and the DAMP 0.1, based on findings in literature [23].The inadequacy of the material model not being able to take strain rates into account other than by the DAMP coefficient, combined with the strain-rates being high during helmet impacts can possibly cause a significant difference in energy

absorption during impact between the real and virtual helmet. A possibility is then to use the material keyword MAT_MODIFIED_CRUSHABLE_FOAM instead since it allows the user to have multiple yield stress-strain curves for different strain-rates [22]. However, no data for the strain-rate dependent behaviour was available and performing material tests for the strain-rate effect of EPS was out of the scope for this project. Strain-rate effects will be further touched on in Chapter 6.5.

In the calculations of the stress in the crushable foam, a constant value for the Young's modulus is used giving an elastic behaviour as seen in equation 4.1, where the stress is denoted by σ_{ij}, E is Young's modulus, $\dot{\varepsilon}_{ij}$ is the strain rate and Δt is the time step.

$$\sigma_{ij}^{trial} = \sigma_{ij}^n + E\dot{\varepsilon}_{ij}^{n+1/2}\Delta t^{n+1/2} \tag{4.1}$$

To regulate the stress so it follows the yield stress-strain curves, the principle stress, $\sigma_i^{trial}, i = 1, 3$, are scaled back to the yield stress as in equation 4.2, where σ_y is the yield stress [20].

$$\sigma_y < |\sigma_i^{trial}| \Rightarrow \sigma_i^{n+1} = \sigma_y \frac{\sigma_i^{trial}}{|\sigma_i^{trial}|} \tag{4.2}$$

An alternative to the crushable foam for the EPS is the material keyword MAT_LOW_DENSITY_FOAM which is suitable for highly compressible isotropic foam undergoing large deformations. The two models are somewhat similar and both require a load curve for the yield stress-strain as input. Where the two instead significantly differ from each other is during the unloading phase. Low density allows for the material to completely recover after loading whilst the crushable foam instead results in very little recovery, closely resembling a material experiencing damage after loading.

4.2.3 Anvil

The anvil was modeled as a rigid steel plate with the use of 1 mm thick shell elements and the MAT_RIGID keyword. The shell element formulation used was the ELFORM=2: Belytschko-Tsay which is chosen by default. The material properties for the steel can be seen in Table 4.2.3.

Table 4.2.3: Material properties for anvil.

Steel anvil	
Density [kg/m^3]	7500
Young's modulus [GPa]	200
Poisson's ratio	0.3

4.2.4 Headform

Similarly to the anvil, the headform was modelled with the MAT_RIGID keyword, however the head uses solid elements with element formulation ELEFORM=1: constant stress solid element. The material used for the headform is magnesium K1A alloy with adjusted density to match the weight of the headform used in the experiments (4.7kg).

Table 4.2.4: Material properties for headform.

Magnesium K1A alloy headform	
Density [kg/m^3]	1153
Young's modulus [GPa]	44.8
Poisson's ratio	0.3

4.2.5 Contact conditions

Defining appropriate contact conditions are essential to get a model that behaves as expected since they are prone to cause instabilities. The model consists of 4 parts (PC shell, EPS foam, headform and anvil) that all, directly or indirectly, interact with each other. The keywords used in LS-DYNA to define the contacts can be seen in Table 4.2.5.

Table 4.2.5: Contact conditions.

CONTACT	PARTS
AUTOMATIC_SURFACE_TO_SURFACE	PC to Anvil
AUTOMATIC_SURFACE_TO_SURFACE	Head to EPS
TIED_SHELL_EDGE_TO_SURFACE_BEAM_OFFSET AUTOMATIC_SURFACE_TO_SURFACE	EPS to PC
INTERIOR	EPS

Headform and EPS

As seen in Table 4.2.5, the LS-DYNA contact keyword between the headform and EPS foam was set to AUTOMATIC_SURFACE_TO_SURFACE. For the definition of the contact, the headform part was set as master and the EPS foam part as the slave since it has higher mesh density. The static coefficient of friction set to 0.3 and dynamic to 0.2. Additionally, for the keyword the optional card A was used with the SOFT option set to be equal to 2.

The AUTOMATIC_SURFACE_TO_SURFACE contact is a penalty based contact meaning that the contact between the parts is treated with a spring-like behaviour. When nodes from the part defined as slave penetrates the master segment, penalty forces proportional to the penetration are applied on the slave nodes to resists further penetration and move them back to the master segments surface [24].

Interior EPS contact

The EPS foam is expected to experience large compressive strains during impact and that densification of the foam will occur, however since the slope of the yield stress-strain curves for the foam were reduced for strains above 0.8, the material will have a more compliant behaviour. This can then cause the foam to invert during high loads causing negative volume elements in LS-DYNA. To counteract the negative volume elements in the EPS foam during large deformations the CONTACT_INTERIOR card was used in LS-DYNA to prevent the solid elements from penetrating themselves [23].

EPS and PC

The keyword TIED_SHELL_EDGE_TO_SURFACE_BEAM_OFFSET was used for the contact between the EPS and PC to tie the nodes of the PC mesh to the surface of the EPS. In the model a small gap existed between the two parts, therefor the offset option for the contact was used since it maintains the offset between the parts and the geometry of the slave side is unaltered. The offset option also switches the tied contact from constrained-based to penalty-based. The beam option allows for force and moment transfer between the PC's shell elements and the EPS's solid elements [24].

In the case that some of the PC nodes fails to tie to the EPS surface, the keyword CONTACT_AUTOMATIC_SURFACE_TO_SURFACE was used to prevent penetration between the parts at untied locations.

PC and anvil

The contact between the PC and anvil was modelled with the CONTACT_AUTOMATIC_SURFACE_TO_SURFACE keyword with the PC as the slave segment and the anvil as the master segment. The static friction coefficient was set to 0.3 and dynamic to 0.2.

4.2.6 Dealing with initial penetrations

When building and setting up the geometry for the model, initial penetrations proved to be a challenge since the parts for the helmet was meshed separately. Initial penetrations were also encountered when trying to fit the headform to the helmet. The CAD models for the EPS and PC originally overlapped which likewise resulted in their mesh overlapping when imported into LS-PrePost. To eliminate most of the initial penetration between the parts, surface nodes of the EPS which were supposed to be in contact with the outer shell were projected onto the 2D elements of the PC shell with an offset of 0.6 mm. This method removed most of the overlapping however problem areas where initial penetration were visible still existed. To further improve the model the Contact Check tool under Model Check in LS-PrePost was used which identifies initial penetrations between contact pairs and tries to move elements to minimise the penetration.

Under the keyword CONTROL_CONTACT the IGNORE flag was set equal to 1. This handles initial or unexpected penetrations between the parts by allowing the initial penetrations to exist. The penetrations are tracked and the contact parameters are adjusted locally, however no nodes are moved nor are any contact forces applied. For additional penetration the program will apply contact forces to prevent further penetration.

4.2.7   Fitting of headform

The headform was placed manually in the helmet as closely to the EPS as possible whilst also trying to avoid penetrations between the headform and EPS. The penetrations that arose were dealt with the Model Check tool mentioned in Chapter 4.2.6. The helmet mounted on the headform can be seen in Figure 4.2.2 where the helmet is placed directly upon the headform with no tilt back or forward. Tilting the helmet backward could possibly result in a model more accurate to the experimental setup, but since the tilt angle was not measured during the experimental tests it was assumed to be zero.

Figure 4.2.2: Helmet mounted onto headform.

4.2.8   Initial and boundary conditions

Instead of simulating the full drop of the helmet and headform, they are given an initial velocity equal to the desired impact velocity for the drop test. This was done by using the INITIAL_VELOCITY_GENERATION keyword in LS-DYNA and giving the parts for the headform, EPS and PC the desired velocity. The displacement and rotation for the anvil's centre of mass was constrained in all directions, completely locking it in place during impact.

Since only half of the helmet was modelled, see Figure 4.2.3, symmetry boundary conditions were applied on the surfaces of the middle cross section. The boundary condition locks translation in the normal direction of the symmetry plane and locks rotation for directions parallel to the symmetry plane.

(a) Front view.

(b) Side view.
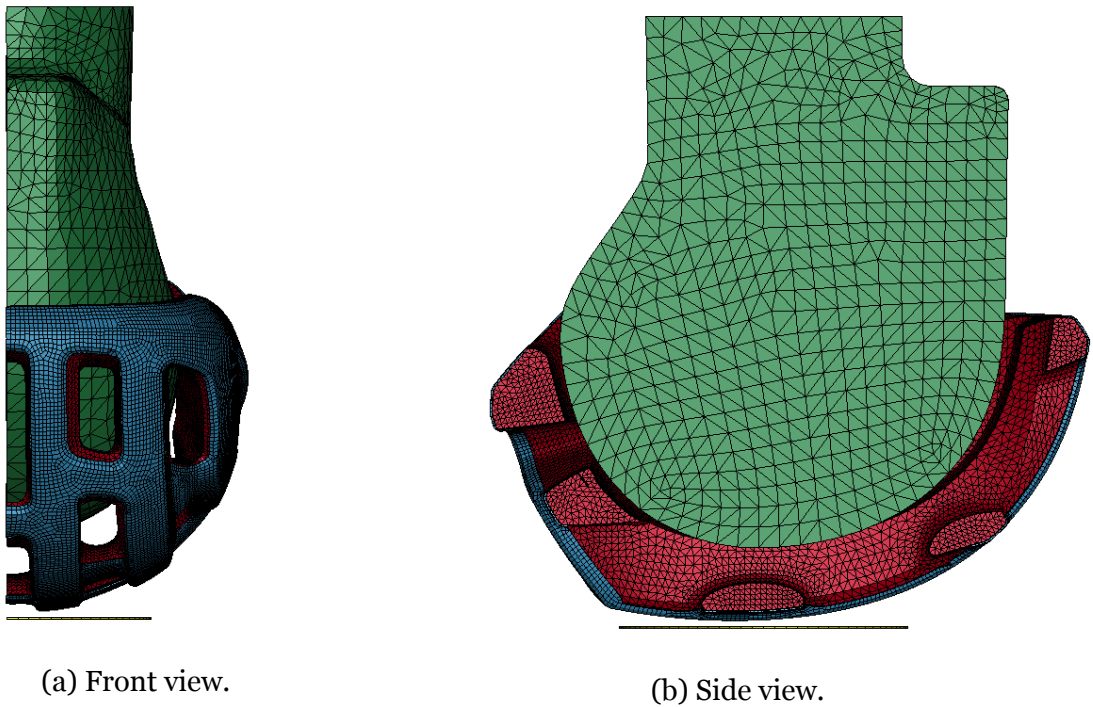
Figure 4.2.3: FE-model with symmetry plane (top impact).

For the back impact case the headform and helmet was rotated 55 degrees as seen in Figure 4.2.4.

(a) Front view.

(b) Side view.
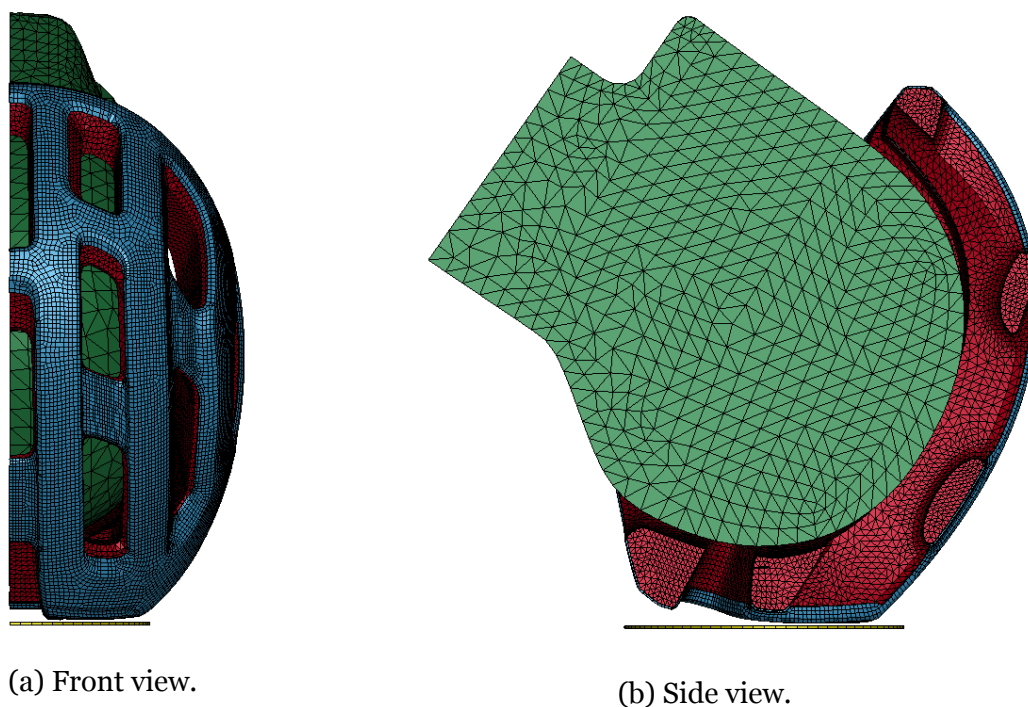
Figure 4.2.4: FE-model with symmetry plane (back impact).

4.2.9 Solver setup and post processing

The FE simulation was solved explicitly, using the SMP single method. The termination time was set to 15 ms, and the time interval between the outputs was chosen to be 0.125 ms. To obtain the peak acceleration value from the impact, the resultant acceleration of the head was plotted against the time in LS-PrePost.

Chapter 5

FE-simulation

In this chapter the results from the FEA is presented, showing the resultant acceleration of the headform, plotted over the impact time. In Figure 5.0.1 the acceleration plot for the FE-model with an impact velocity of 5.42 m/s and different EPS foam densities can be seen. In the figure, the slope during the initial part of the impact gets steeper with a higher density, and that the peak acceleration increases as well. For the lower densities a load retardation occurs around 4 ms, whereas the 100 gpl density shows a plateau rather than a peak.
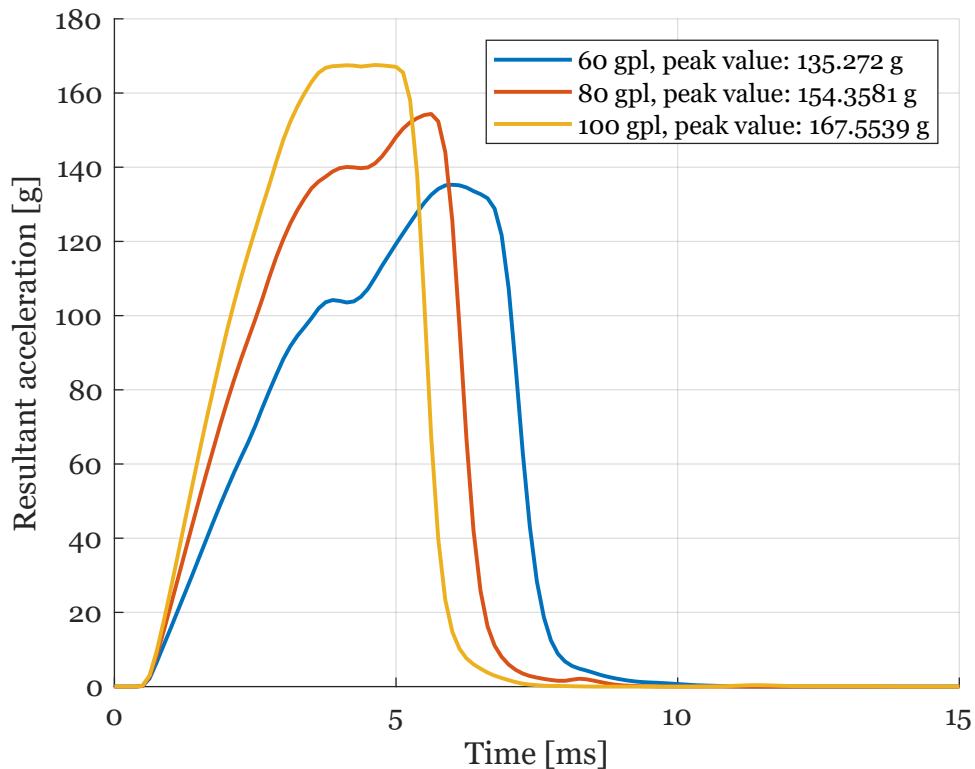
Figure 5.0.1: Acceleration vs time plots of 60 gpl, 80 gpl and 100 gpl for crown impact at 5.42 m/s.

The crown impact of the helmet simulation with a density of 60 gpl is plotted for all the velocities in Figure 5.0.2. The steepness of the curve increases with the velocity, as the impact time decreases slightly. The shape of the curve changes drastically for the velocity of 7.70 m/s, where the peak of the curve takes on a pointier shape, compared to the cases with lower velocities where a load dip is more distinct.
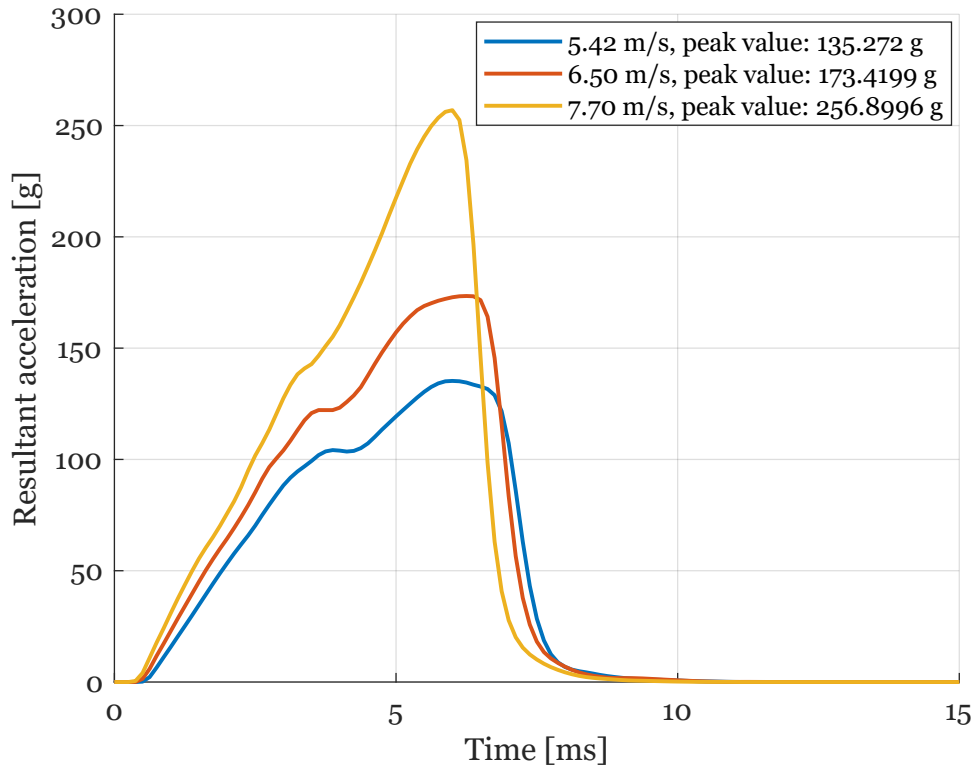
Figure 5.0.2: Crown impact for EPS with density 60 gpl and impact velocities 5.42, 6.50 and 7.70 m/s.

In Figure 5.0.3 the plots of the back impact simulations for the case of 5.42 m/s for all the densities are shown. No clear load dip is shown in these plots, however the slope is not even. The steepness increases with the density, as well as the peak acceleration.
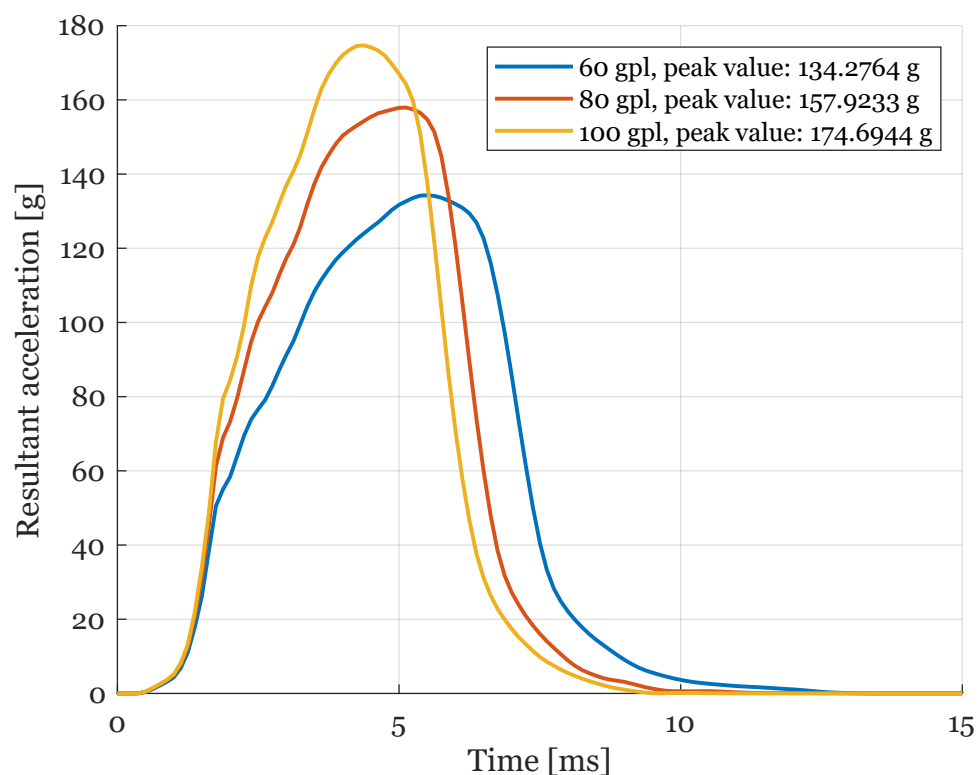
Figure 5.0.3: Acceleration vs time plots of 60 gpl, 80 gpl and 100 gpl for back impact at 5.42 m/s.

The velocity dependence of the back impact for the helmet with density 60 gpl is shown in Figure 5.0.4. The higher velocity yields a higher peak acceleration, as well as a different shape of the curve.
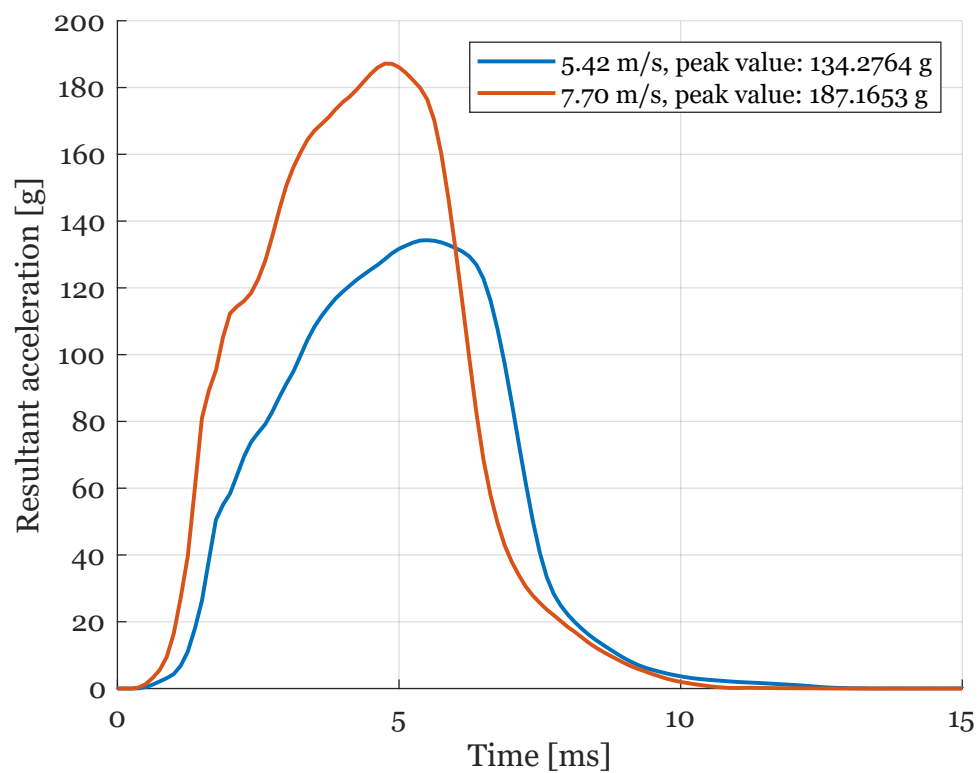
Figure 5.0.4: Back impact for EPS with density 60 gpl and impact velocities 5.42 and 7.70 m/s.

Chapter 6

FE-parametric study

After the original setup of the helmet in LS DYNA had been simulated for all the cases, a parametric study was made for material parameters such as the dampening coefficient DAMP, the tensile stress cutoff TSC, and the shell thickness, as well as Young's modulus of the PC shell. In addition to this, a strain rate dependent material was interpolated using a strain rate power law, and the EPS foam was thickened with 5 and 10 mm. All the parameter changes were made for the simulation setup with the density of 60 gpl and the velocity 5.42 m/s.

6.1   Tensile stress cutoff

As mentioned earlier, the material model for MAT_CRUSHABLE_FOAM entails an optional parameter for Tensile stress cutoff , TSC. In the original setup this parameter was set to 0.1 MPa, a value found in literature. The TSC was varied between 0.01 and 10 MPa, as seen in Figure 6.1.1. A larger value of the TSC leads to a higher peak acceleration, as well as a steeper load curve. The load dip is prevalent in all curves, except for when the TSC is set to 0.01 MPa.
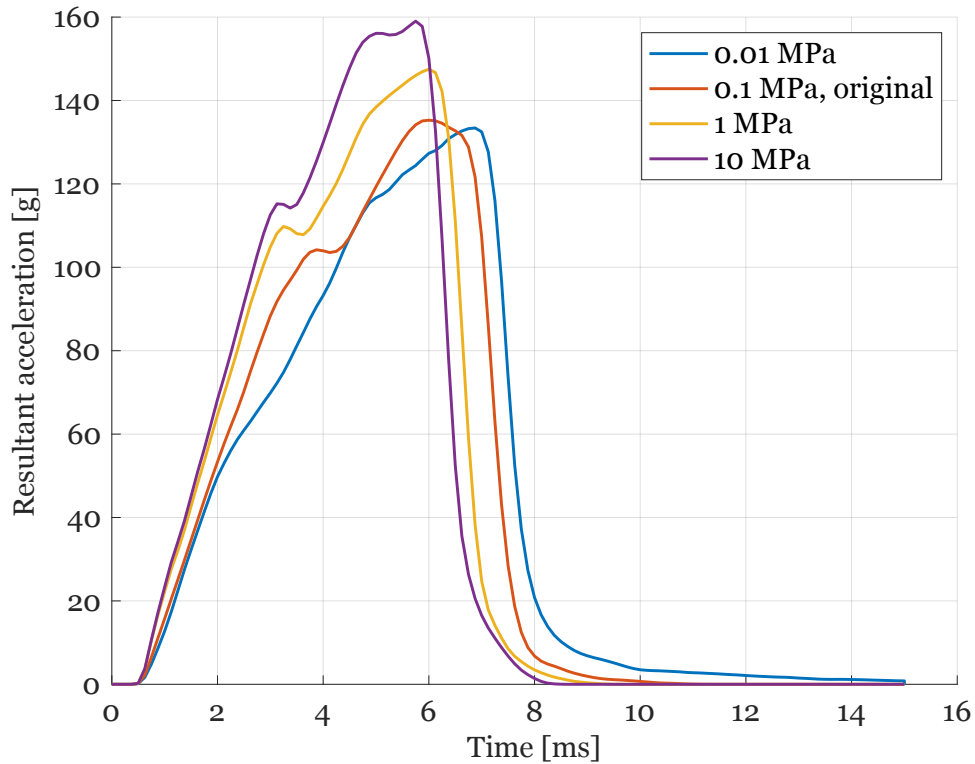
Figure 6.1.1: Varying Tensile Stress Cutoff.

6.2 Dampening coefficient

The next parameter to be varied was the dampening coefficient DAMP, which is the only way to account for strain rate dependency in the material model for MAT_CRUSHABLE_FOAM. It is recommended to use a value between 0.05 and 0.5. As seen in Figure 6.2.1, the change of the dampening coefficient makes for a minimal difference in the peak acceleration, as well as the shape of the curve.
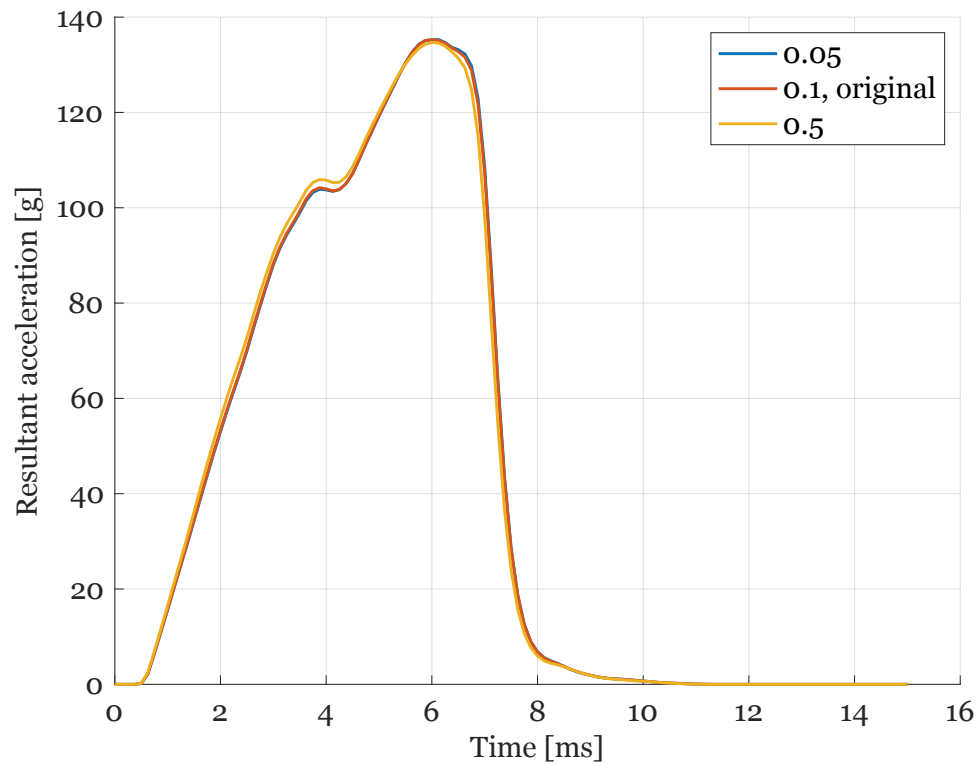
Figure 6.2.1: Varying DAMP.

6.3 PC shell thickness

The thickness of the PC shell was first increased by a factor two, and then it was divided by two. The thickness was then further decreased to see the behaviour of the helmet with an even thinner shell, as well as with no PC shell at all. This is plotted in Figure 6.3.1, where it can be seen that the load dip is more evident for a thicker PC shell, and does not occur for a very thin or non-existent PC shell. The impact time increases with a thinner PC shell, and the slope flattens out.
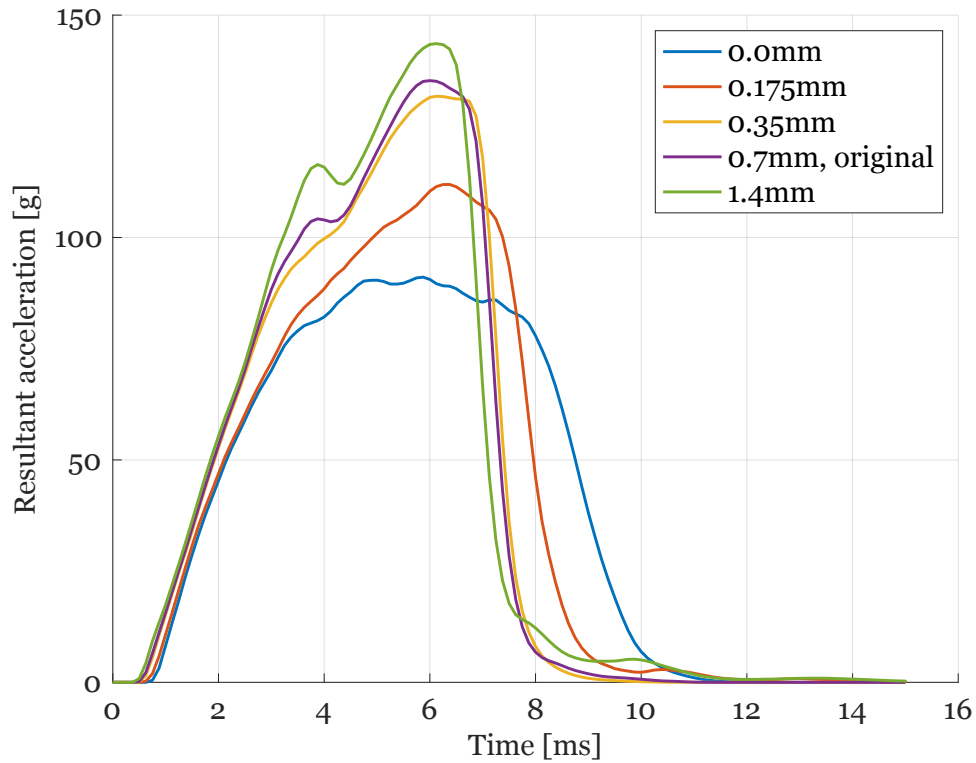
Figure 6.3.1: Varying the thickness of the PC shell.

6.4 Young's modulus of the PC shell

The Young's modulus of the PC material was increased and decreased by 10%, pictured in Figure 6.4.1. A slight increase of peak acceleration can be seen for the curve with a Young's modulus of 2.42 GPa, as well as a small decrease of peak acceleration for the curve with a Young's modulus 1.98 GPa, but the differences are barely discernible.
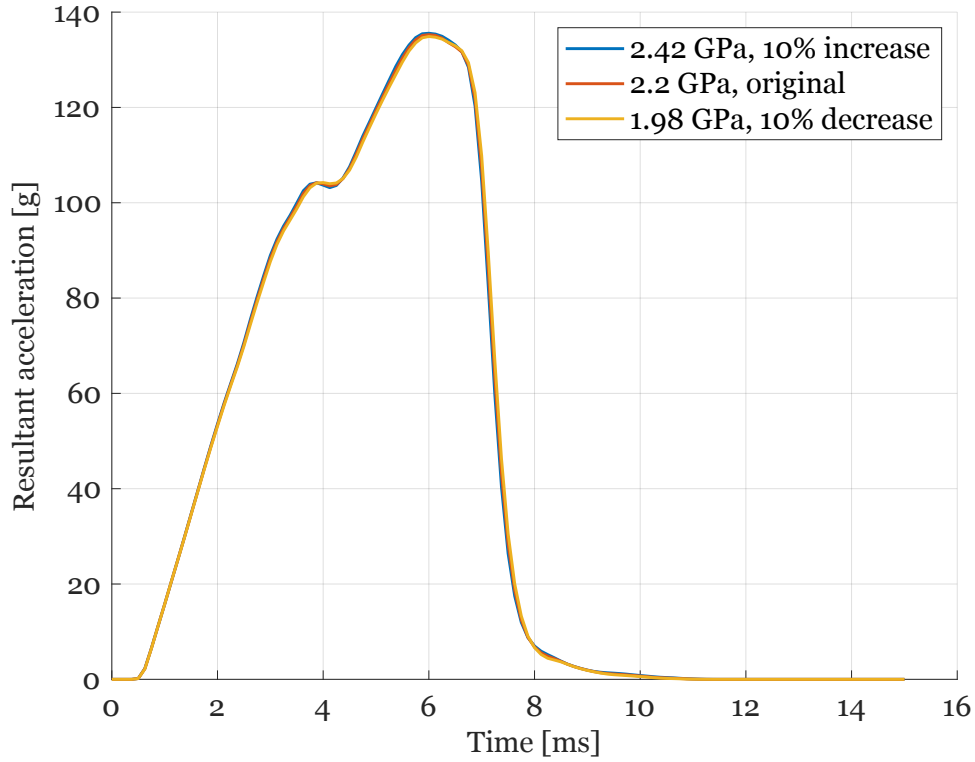
Figure 6.4.1: Varying the Young's modulus of the PC material.

6.5 Strain-rate dependency

To try to capture the strain-rate dependent behaviour of the material, the power law seen in equation 6.1 is used to modify the EPS's yield-stress strain curve. In the equation, σ_y is the strain-rate dependent yield stress, $\sigma_{y,0}$ is the quasi-static yield stress, $\dot{\varepsilon}_0$ is the quasi-static strain rate and $\dot{\varepsilon}$ is the strain rate the material experience [25]. For the values of the quasi-static parameters in the equation, the stress-strain data obtained from POC was used. In the material test data, the quasi-static strain-rate was $\dot{\varepsilon}_0 = 0.02 \text{ s}^{-1}$.

$$\sigma_y = \sigma_{y,0} \left(\frac{\dot{\varepsilon}}{\dot{\varepsilon}_0} \right)^{n(\varepsilon)} \tag{6.1}$$

The exponent n is a function of the strain, see equation 6.2. The values for a and b were chosen until a satisfactory behaviour for the curves was obtained. The values used were $a = 0.12$ and $b = 0.08$.

$$n = a + b\varepsilon \tag{6.2}$$

The resulting stress-strain curves for the 60 gpl foam at different strain-rates can be

seen in Figure 6.5.1.
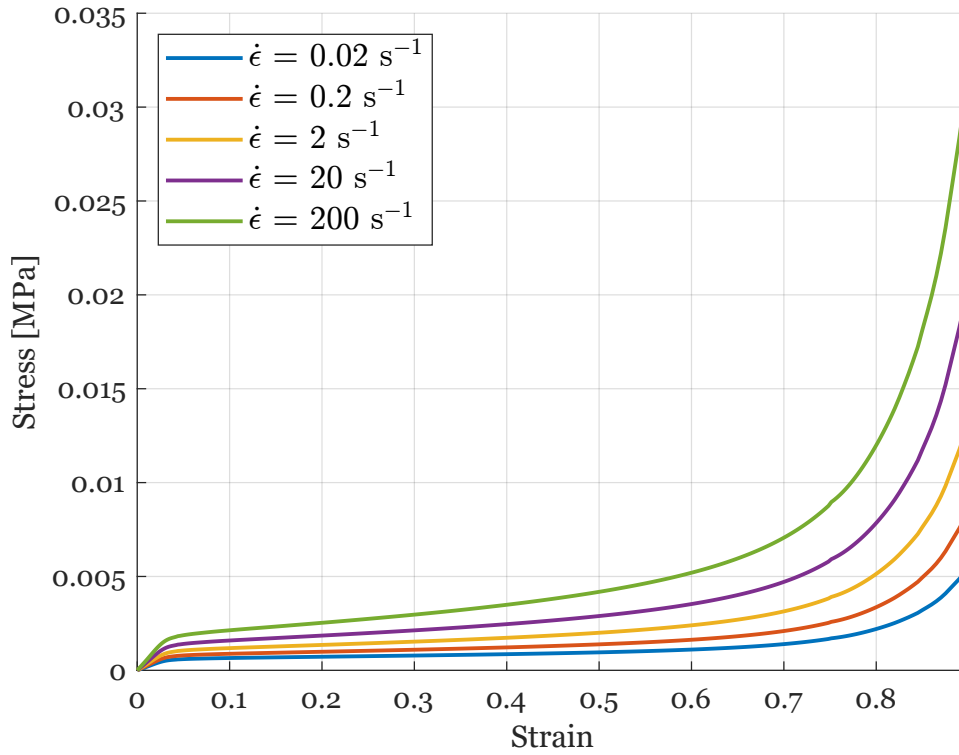
Figure 6.5.1: Stress-strain curves for 60 gpl EPS foam with strain-rate dependent behavior.

To implement the new strain-rate dependent material behaviour of the foam in the FE-model the MAT_MODIFIED_CRUSHABLE_FOAM keyword was used. The material model is similar to the crushable foam but allows for inclusion of strain-rate effects by defining multiple yield stress-strain curves with an assigned associated strain-rate.

In Figures 6.5.2 to 6.5.4 the effect from including a strain-rate dependent material behaviour on the resultant acceleration during impact can be observed. A initial stiffer response to the impact can be seen with the slope being steeper during the beginning. For most cases the peak resultant acceleration is reduced with the exception of the case with foam density 100 gpl and impact velocity 5.42, seen in Figure 6.5.4, where the peak instead occurs earlier and sees a small increase. The inclusion of the strain-rate effect also display the largest influence for the cases with higher impact velocity since the deviation between the curves increases as the velocity increases. Furthermore, during unloading the modified curves remain similar to the originals. This suggests that the strain-rate dependent behaviour only bears significance on the initial part of impact.
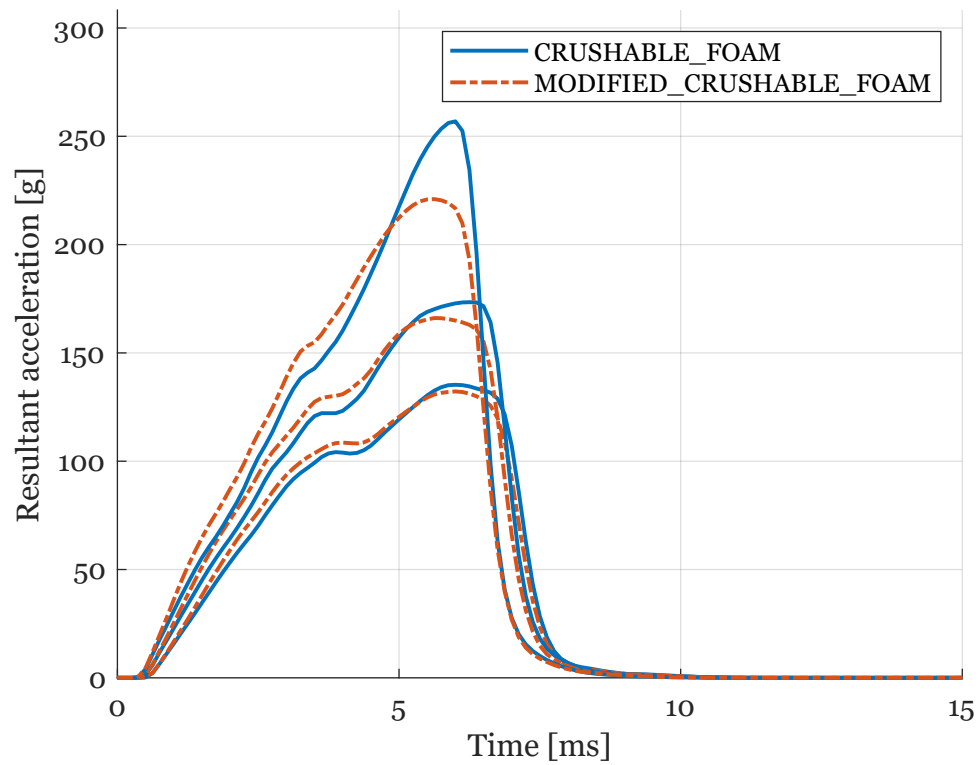
Figure 6.5.2: Inclusion of strain-rate effects for 60 gpl, crown impact for velocities 5.42/6.50/7.70 m/s.
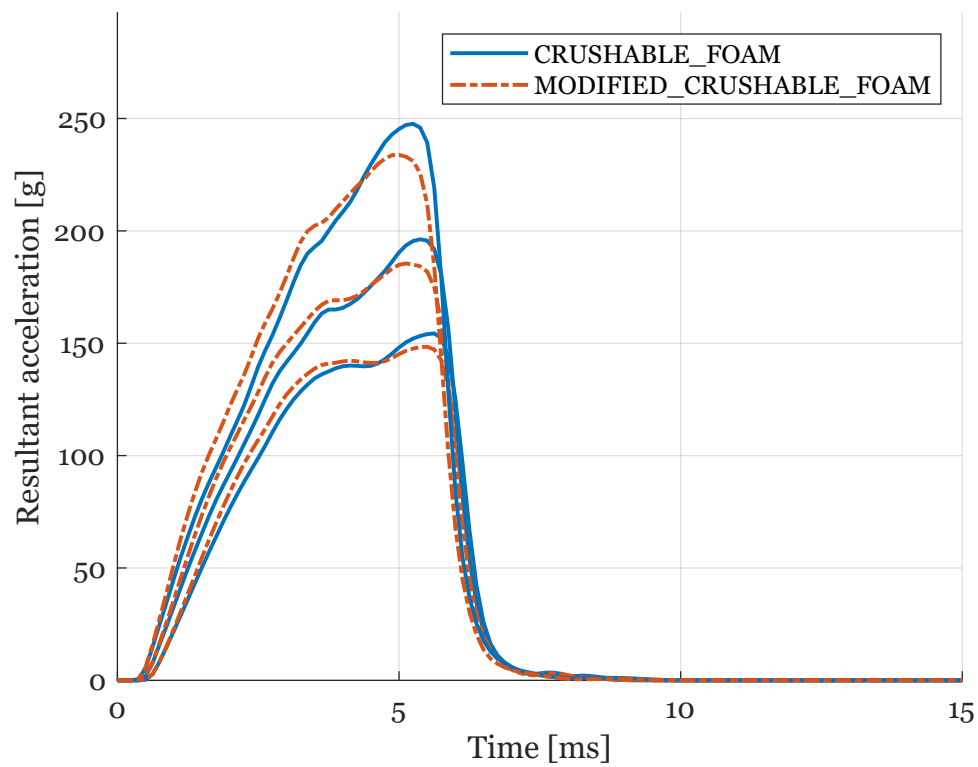
Figure 6.5.3: Inclusion of strain-rate effects for 80 gpl, crown impact for velocities 5.42/6.50/7.70 m/s.
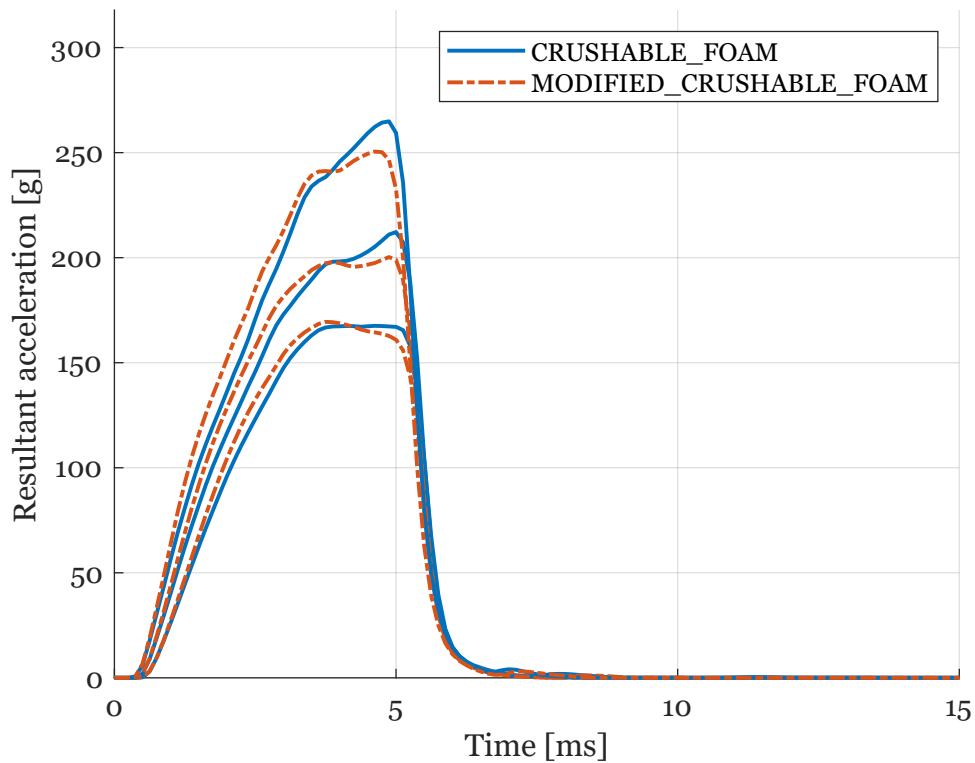
Figure 6.5.4: Inclusion of strain-rate effects for 100 gpl, crown impact for velocities 5.42/6.50/7.70 m/s.

6.6 EPS thickness

To improve the impact absorption capabilities of the helmet, a reasonable solution would be to make increase the amount of EPS in the helmet. Therefore, the CAD model was modified to investigate this by increasing the EPS thickness by 5 mm and 10 mm, see Figure 6.6.1.

The helmets with thicker EPS was then subjected to the crown impact for the three velocities, see Figures 6.6.2, 6.6.3 and 6.6.4. In the figures the helmet with increased thickness display a reduction in peak acceleration with the peak also occurring later. The figures also show how the reduction of acceleration between the geometries gets lower as the thickness increases.

Additionally, the increased thickness helps with preventing the helmet from bottoming out at higher loads. This is best observed in Figure 6.6.4 where the design with the original thickness results in a sharp high peak, whereas the slope of the curves with the thicker designs is lower resulting in a more blunted shape and a decrease in peak acceleration.
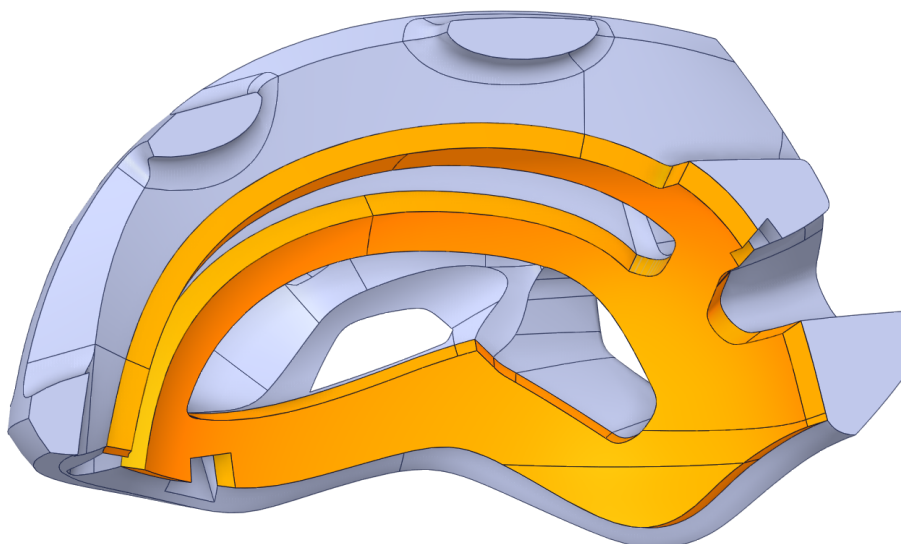
Figure 6.6.1: CAD model with thicker EPS.
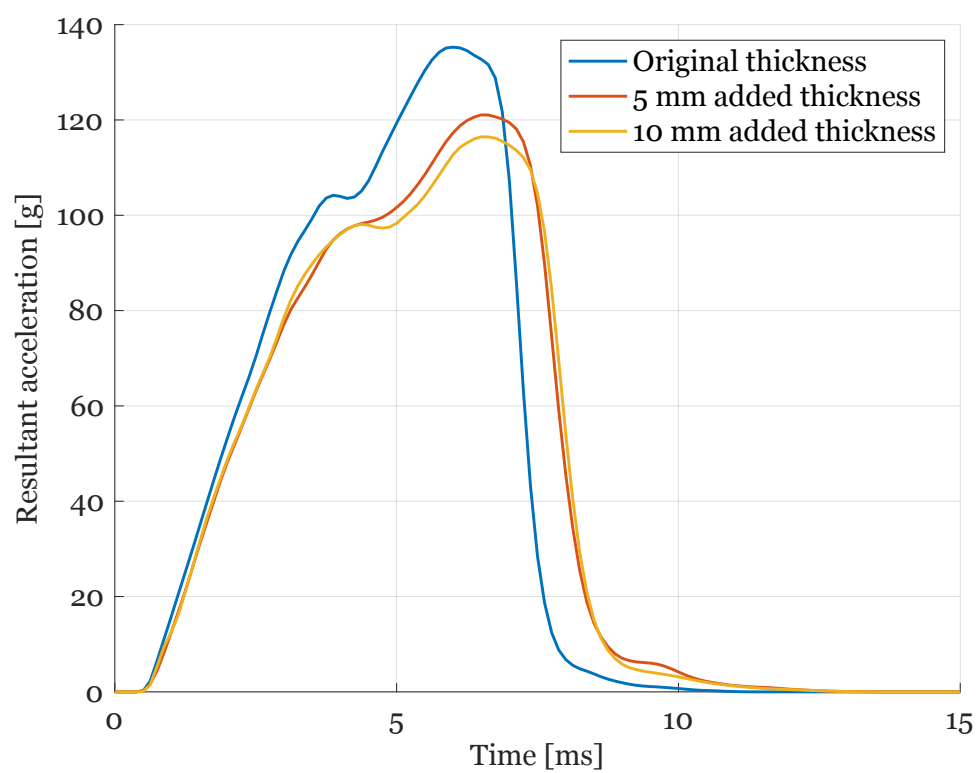
Figure 6.6.2: Varying the EPS thickness for the case of 60 gpl and 5.42 m/s.
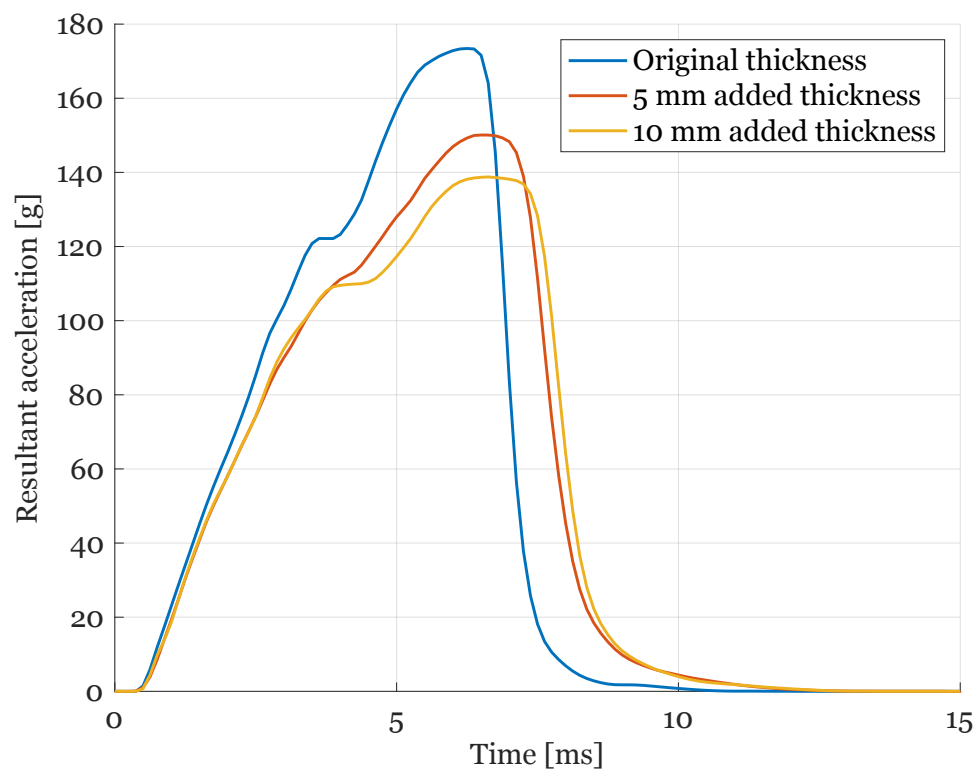
Figure 6.6.3: Varying the EPS thickness for the case of 60 gpl and 6.50 m/s.
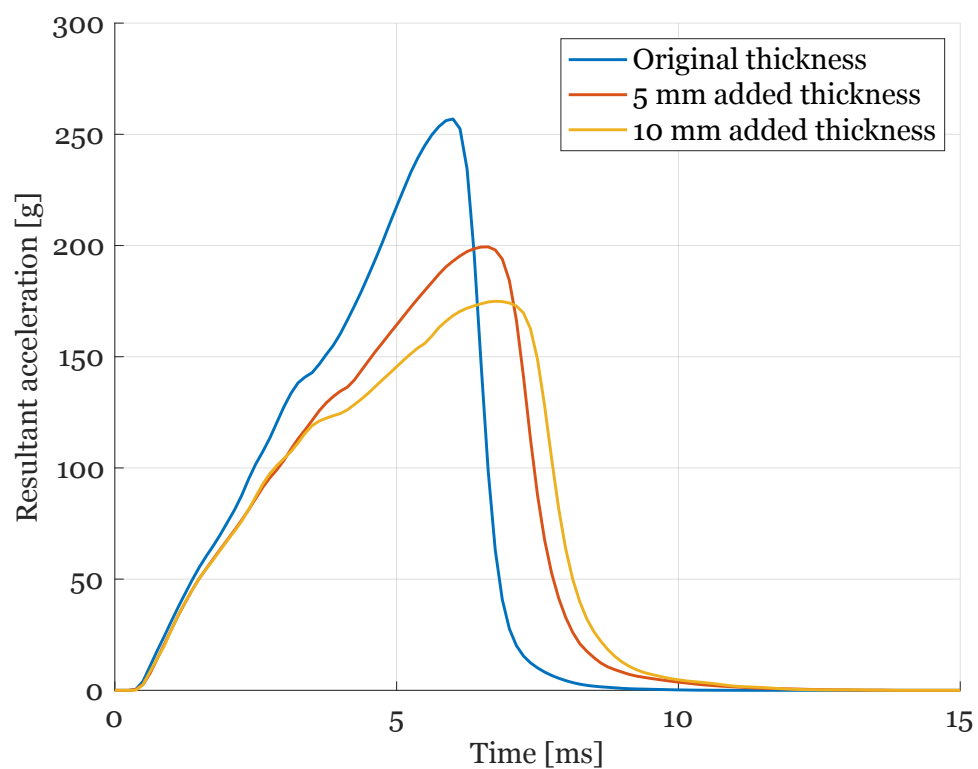
Figure 6.6.4: Varying the EPS thickness for the case of 60 gpl and 7.70 m/s.

Chapter 7

Evaluations and comparisons

This chapter is a zoom out of all results, where all previous work is summarised and evaluated. The experimental result will be compared against the FE-simulation and the parameters from the FE-parametric study that have a great impact will be presented.

7.1 Experiment & Simulation results

In Figure 7.1.1 to 7.1.3, experimental results of the 5.42 m/s velocity crown impacts are plotted against the results from simulations, for all the densities. The figures displays a discrepancy between the two different methods in both the shape of the curves and for the value of the peak acceleration. The difference in shapes for the curves seem to mainly come from the difference in slope steepness during the initial increase of acceleration and the unloading behaviour after the peak. For all crown impact cases the curve for the simulation have less of a steep initial slope with a much faster unloading behaviour. The peak acceleration values do however have similar values despite of these discrepancies in shape, with the difference in peak values seemingly growing smaller for the higher densities.
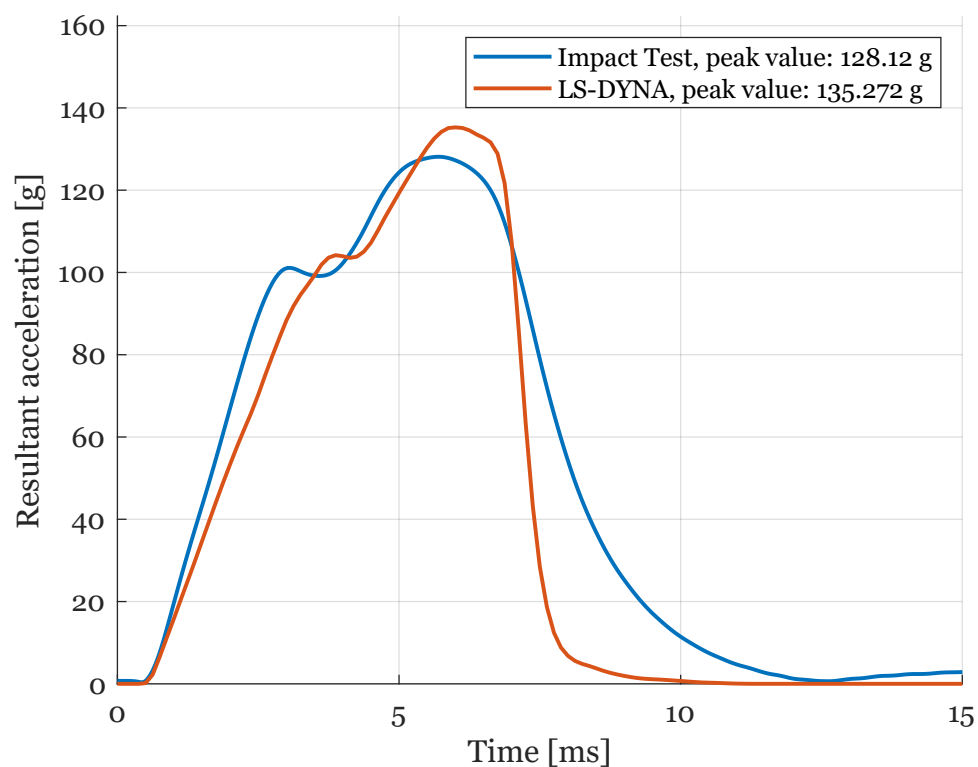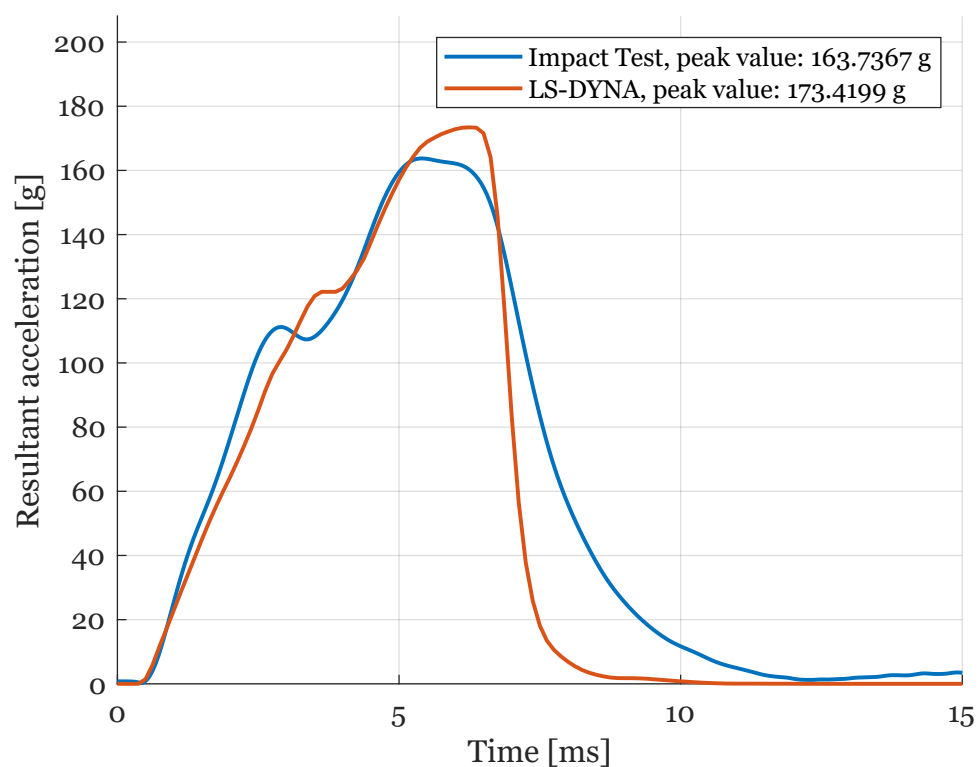
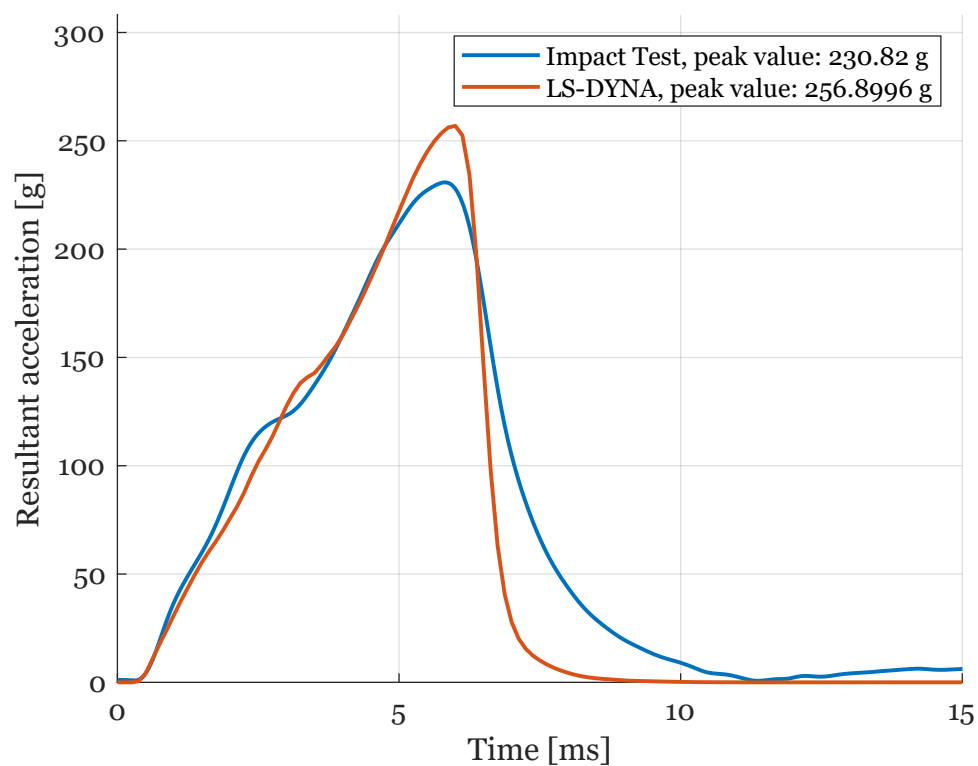Figure 7.1.1: Experimental and simulation results for crown impact with density 60 gpl and velocity 5.42 m/s.
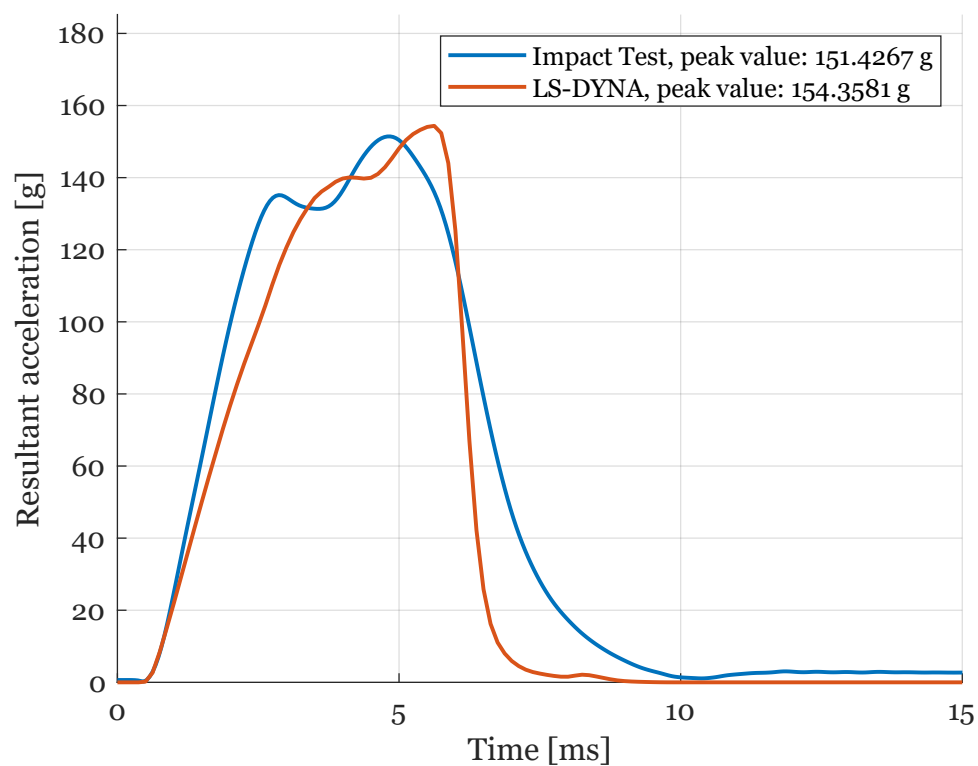
Figure 7.1.2: Experimental and simulation results for crown impact with density 80 gpl and velocity 5.42 m/s.
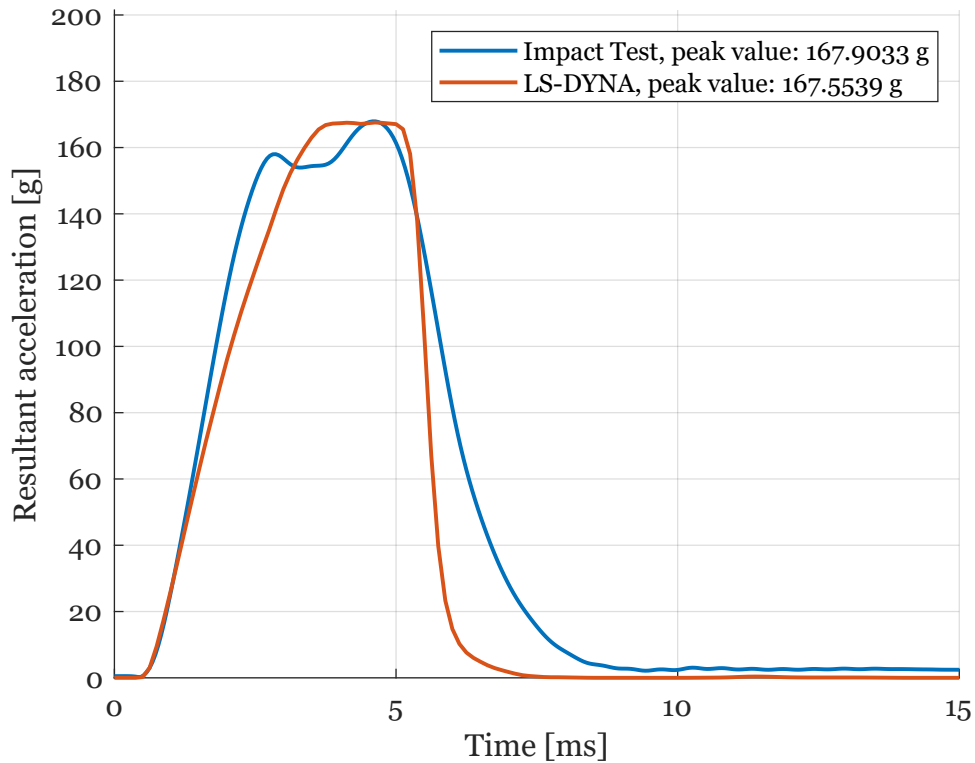
Figure 7.1.3: Experimental and simulation results for crown impact with density 100 gpl and velocity 5.42 m/s.

Comparing the experimental results and FE-analysis for higher velocities results in the curves seen in Figures 7.1.4 and 7.1.5 for the 60 gpl density helmet, the curves for the other densities can be found in appendix D. These figures together with the curves from the 5.42 m/s case with density 60 gpl, see Figure 7.1.1, show how the discrepancy between the peak values increases for the higher velocities.

Figure 7.1.4: Experimental and simulation results for crown impact with density 60 gpl and velocity 6.5 m/s.

Figure 7.1.5: Experimental and simulation results for crown impact with density 60 gpl and velocity 7.7 m/s.

The behaviour of the load dip is also different between the experimental and simulation curves for the crown impact cases. One can discern a load dip at around 3 ms for all the experimental crown impact tests, and a load retardation is visible in some of the simulation results as well. However, it occurs shortly after the dip in the experiment curve, possibly as a consequence of the lower initial stiffness. The load dip in the curves for the simulation, also seems to be more well defined for the lower densities and velocities. In the case of the simulation with density 100 gpl and impact velocity 5.42 m/s, see Figure 7.1.3, the load dip is missing whilst the experimental curve still shows the load dip.

From comparing the results it becomes apparent that for most cases of crown impact, the FE-analysis results a higher peak acceleration value than the one obtained from the experiments. The simulation then shows a tendency to overestimate the peak acceleration value for crown impact.

Similar load dips to the ones seen in crown impact can be observed in the experimental curves for the cases of back impact, see Figures 7.1.6 to 7.1.9. Unlike the cases for crown impact, the back impact displays multiple irregular load dips which might be the cause of noisy measurements. Nonetheless the curves still show some consistency with a load dip occurring at circa 2 ms for each experimental curve. These load dips are however not as prominent in the results for the FE-simulation with it being more visible for higher impact velocities. The initial slope of the curves from simulation are also here not as steep as for the experimental curves, however, the unloading behaviour seem to have a better match. Again as for the case of crown impact, the discrepancy for the peak acceleration increases with the increase in velocity for back impact, but, on the contrary, for the cases of back impact the FE-analysis gives smaller peaks than the experimental results. For back impact the simulation then instead shows a tendency to underestimate the peak acceleration value.
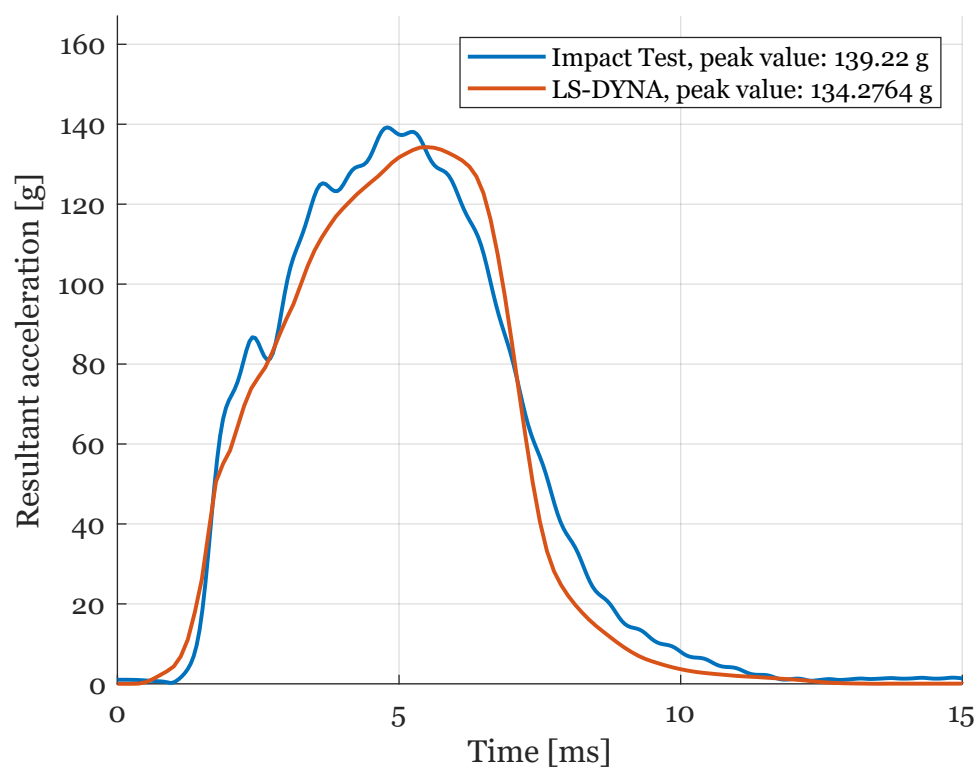
Figure 7.1.6: Experimental and simulation results for back impact with density 60 gpl and velocity 5.42 m/s.
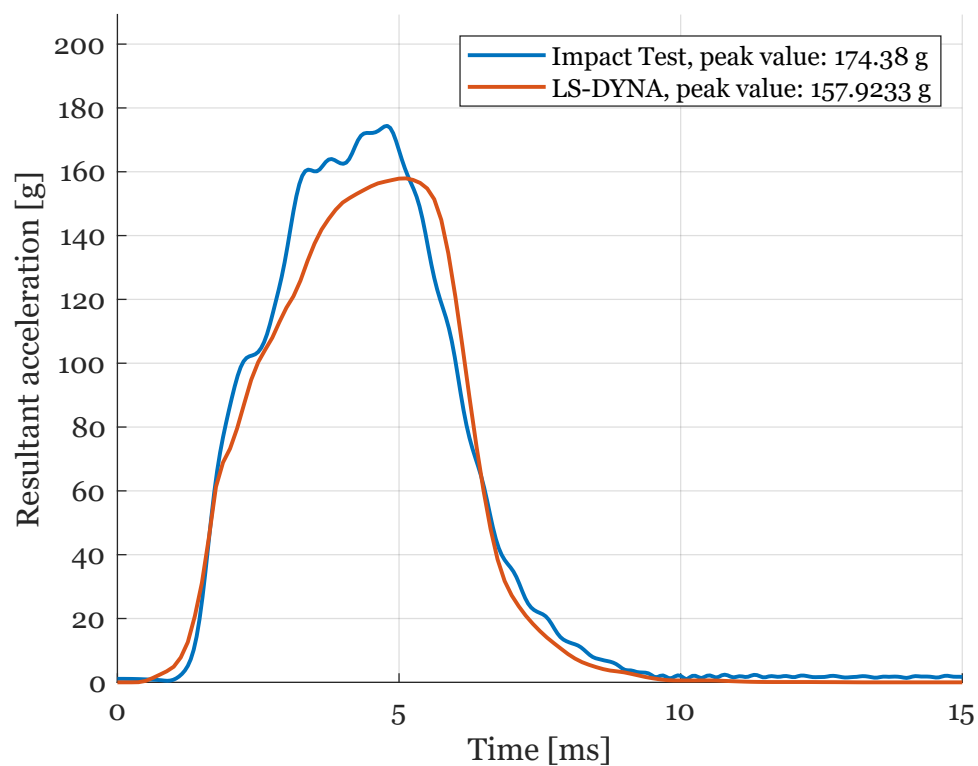

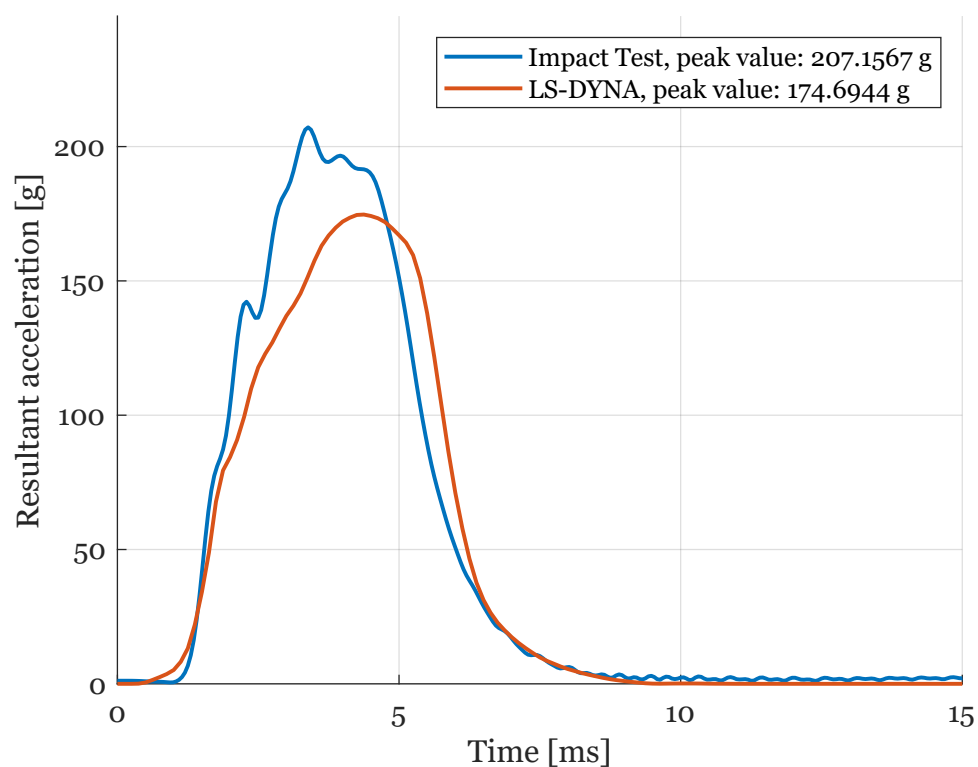Figure 7.1.7: Experimental and simulation results for back impact with density 80 gpl and velocity 5.42 m/s.

Figure 7.1.8: Experimental and simulation results for back impact with density 100 gpl and velocity 5.42 m/s.
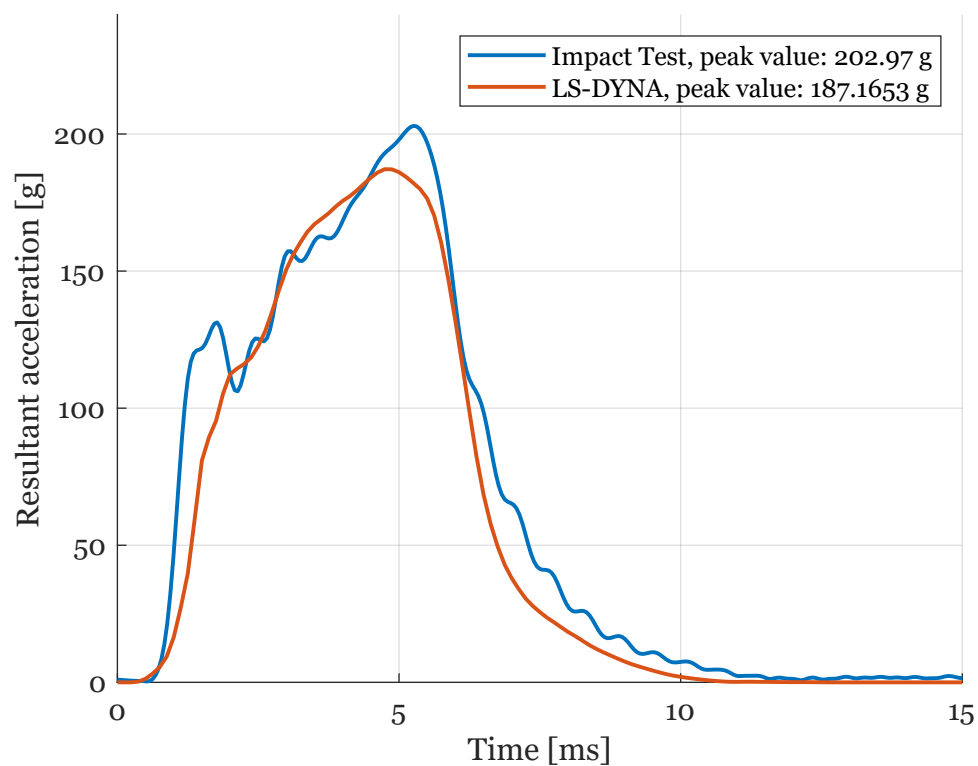

Figure 7.1.9: Experimental and simulation results for back impact with density 60 gpl and velocity 7.7 m/s.

7.2   Parametric study results

The parameters that had a great impact on the peak acceleration value were the tensile stress cutoff, the PC shell thickness, the strain rate dependent material, and the EPS thickness.

The strain rate dependency of the EPS was investigated in Chapter 6.5, where the material was changed from CRUSHABLE_FOAM, the material originally used in the simulations, to MODIFIED_CRUSHABLE_FOAM. The results showed a steeper initial curve, as well as a lower peak acceleration value, compared to the CRUSHABLE_FOAM material which did not take strain rates into account, other than by a dampening coefficient. The dampening coefficient DAMP was parameterised in 6.2, and showed to not have any great effect on nether the initial slope, nor the peak acceleration value.

When varying the tensile stress cutoff, in Chapter 6.1, one could see that the position of the load dip, as well as the slope of the curve, changed with the value of the TSC, where a larger TSC value generated a steeper curve and an earlier load dip. However, a larger TSC value also led to a greater peak acceleration. It is interesting that a parameter that changes the behaviour of the EPS foam in tension has such a great impact on the resultant acceleration during an impact test.

The thickness of the EPS showed to have a grand effect on the peak acceleration score of the helmet impact, as seen in Chapter 6.6. When adding 5 mm of extra thickness, the acceleration greatly decreases compared to the original thickness. However, when adding 10 mm of extra thickness, the peak acceleration does not drop that much more compared to the 5 mm helmet, which suggests that maybe not all material is compressed during the impact of the 10 mm helmet.

The Young's modulus of the PC shell did not make a noticeable change to the shape of the curve, nor the peak acceleration, as seen in 6.4. In Chapter 6.3, when changing the thickness of the PC shell, that proved to have a larger impact on the peak acceleration. A thin, or non-existent, PC shell greatly decreased the acceleration, and this suggests that perhaps helmets should be designed without PC shells. This might, however, be a trend that is seen only in the simulation, as no experimental tests have been performed on this.

Chapter 8

Discussion

From comparing the experimental results with the simulation we can observe that they show some discrepancies between their results, with the FE-model having a more compliant response in the beginning of the impact with less of a steep slope during the initial increase of acceleration. This might suggest that the helmet in FE-model is more compliant than the real one used in the experimental tests. The more compliant response could be a consequence of simplifying the helmet model by removing the inner details of the EPS. Another possibility is that the MAT_CRUSHABLE_FOAM material model is inadequate to capture the behaviour of the foam during impact. As seen in the parametric study, when the TSC value was increased or the strain-rate dependent material included by changing the material model to MAT_MODIFIED_CRUSHABLE_FOAM, a more similar shape of the acceleration curves from the simulation were obtained with a steeper initial slope. These two parameters influence more than only the slope of the curve, for instance, the peak value. Since the FE-model appeared to overestimate the peak acceleration for crown impact, increasing the TSC value to match the slope would then increase the discrepancy between the peak values. Instead the strain-rate dependent material model would be better suited for crown impact since it both increased the slope and lowered the peak value. To the contrary, for back impact, where the FE-model had the tendency to underestimate the peak value, the increased TSC value would then instead decrease the difference between the experimental results and simulation. These contradicting behaviours depending on impact case makes it difficult to draw a conclusion on how to improve the model with these two parameters. It is possible that the current FE-model still is missing critical aspects of the real impact cases, causing these over-and underestimations. However, despite the discrepancies seen in

the results, the model is still able to produce results relatively accurate to experimental tests.

The difference in the unloading behaviour between the FE-model and experiment, mainly for crown impact, is most likely explained by the material model used in LS-DYNA. As mentioned in Chapter 4.2.2, the crushable foam material model has fully elastic unloading, and since the elastic zone for the foam only makes up a small portion of the stress-strain curve, it results in a minimal recovery of the material after the peak load, giving a much faster decrease in resultant acceleration. Since we primarily study the peak acceleration, the question that then arises is if the unloading behaviour even is of importance.

The TSC value has shown to have a large impact on the peak acceleration score, as well as the steepness of the curve. It is interesting that a parameter that controls the properties of the EPS foam in tension has such a great effect during a drop test. This suggests that perhaps there is some tension in the material at some point during the simulation, and perhaps it is correlated to bending of the EPS, and the load dip phenomenon. The load dip shows up in both the experimental test curves, as well as in the simulations. From the experimental results one can see that when the load dip is more prominent, the peak acceleration score is lower, which may indicate that it is something that one would want to design a helmet to have, since it dissipates a lot of the impact energy. However, the parametric study done in LS-DYNA suggests that the load dip comes from the PC shell, and that a helmet with no PC shell at all will have the lowest peak acceleration value. While this is yet to be investigated through experimental tests, the PC shell serves a purpose for the helmet as it distributes loads, and prevents sharp objects from penetrating the EPS. The EPS is a brittle material and will most likely crack during impact if it is not covered by the PC shell.

Chapter 9

Conclusions

The conclusions from this thesis are:

- FE simulations can approximate the peak acceleration score of linear impact tests and be used to investigate helmet design parameters

- The stiffness of the load curve and the peak acceleration increases with density, seen in the experimental tests, as well as in the simulations

- The simulations suggest that the peak acceleration decreases with the thickness of the EPS

- The simulations further suggest that the load dip phenomenon increases with a thicker PC shell

Chapter 10

Future work

Some suggestions for future work ideas:

- Investigate load dip phenomenon further

- Perform experimental tests with thicker EPS

- Try other material models, with real strain rate dependent data

- Perform experimental tests with thinner PC shell

- Simulate more complex impact cases, e.g. with kerbstone anvil or oblique impact

Bibliography

[1]   Thompson, Robert S, Rivara, Frederick P, and Thompson, Diane C. "A case-control study of the effectiveness of bicycle safety helmets". In: *New England journal of medicine* 320.21 (1989), pp. 1361–1367.

[2]   Connor, Thomas A, Meng, Shiyang, Zouzias, Dimitris, Burek, R, Cernicchi, A, De Bruyne, G, Gilchrist, M, Halldin, P, and Ivans, J. "Current standards for sports and automotive helmets: a review". In: *Ref. Ares* 3151745 (2016), pp. 1–42.

[3]   Milne, G, Deck, C, Bourdet, N, Carreira, RP, Allinne, Q, Gallego, A, and Willinger, Rémy. "Bicycle helmet modelling and validation under linear and tangential impacts". In: *International journal of crashworthiness* 19.4 (2014), pp. 323–333.

[4]   Alam, Firoz, Chowdhury, Harun, Elmir, Zakaria, Sayogo, Andika, Love, James, and Subic, Aleksandar. "An experimental study of thermal comfort and aerodynamic efficiency of recreational and racing bicycle helmets". In: *Procedia Engineering* 2.2 (2010), pp. 2413–2418.

[5]   Mustafa, Helmy, Pang, Toh Yen, Perret-Ellena, Thierry, and Subic, Aleksandar. "Finite element bicycle helmet models development". In: *Procedia Technology* 20 (2015), pp. 91–97.

[6]   Ramirez, BJ and Gupta, V. "Evaluation of novel temperature-stable viscoelastic polyurea foams as helmet liner materials". In: *Materials & Design* 137 (2018), pp. 298–304.

[7]   Shuaeib, FM, Hamouda, AMS, Hamdan, MM, Umar, RS Radin, and Hashmi, MSJ. "Motorcycle helmet: Part II. Materials and design issues". In: *Journal of materials processing technology* 123.3 (2002), pp. 422–431.

[8]   *Ventral air MIPS*. URL: https://www.pocsports.com/collections/cycling-helmets-road/products/ventral-air-mips?variant=41480991703192.

[9]   Halldin, Peter. *Energy Absorption*. University Lecture. 2016. URL: `https://kth.instructure.com/courses/3584/files/548567/download?verifier=GDYtug79zNo6nCUvlmDPzJgNjSjLoitLnm83tog8&wrap=1`.

[10]   Sports, POC. *Ventral Air MIPS*. Website. 2022. URL: `https://www.pocsports.com/products/ventral-air-mips?variant=41480992194712`.

[11]   Landro, L., Sala, Giuseppe, and Olivieri, Daniela. "Deformation mechanisms and energy absorption of polystyrene foams for protective helmets". In: *Polymer Testing* 21 (Apr. 2002), pp. 217–228. DOI: `10.1016/S0142-9418(01)00073-3`.

[12]   Croop, Brian and Lobo, Hubert. "Selecting Material Models for the Simulation of Foams in LS-DYNA". In: (Jan. 2009).

[13]   Ling, Chen, Ivens, Jan, Cardiff, Philip, and Gilchrist, Michael D. "Deformation response of EPS foam under combined compression-shear loading. Part II: High strain rate dynamic tests". In: *International Journal of Mechanical Sciences* 145 (2018), pp. 9–23.

[14]   Tahir, Muhammad Naeem and Hamed, Ehab. "Effects of temperature and thermal cycles on the mechanical properties of expanded polystyrene foam". In: *Journal of Sandwich Structures & Materials* 24.3 (2022), pp. 1535–1555.

[15]   Cernicchi, A, Galvanetto, U, and Iannucci, L. "Virtual modelling of safety helmets: practical problems". In: *International journal of crashworthiness* 13.4 (2008), pp. 451–467.

[16]   LS-DYNA. *What are the differences between implicit and explicit?* URL: `https://www.dynasupport.com/faq/general/what-are-the-differences-between-implicit-and-explicit`.

[17]   Standardization. Technical Committee CEN/TC 158" Head Protection, European Committee for. *Helmets for Pedal Cyclists and for Users of Skateboards and Roller Skates*. BSI Standards Limited, 2012.

[18]   Towner, Elizabeth, Dowswell, Therese, Burkes, Matthew, Dickinson, Heather, Towner, John, and Hayes, Michael. *Bicycle helmets: review of effectiveness (No: 30)" report commissioned by the UK Department for Transport*. 2002.

[19]   Teng, Tso, Liang, Cho-Liang, and Nguyen, Van Hai. "Development and validation of finite element model of helmet impact test". In: *Proceedings of the Institution of Mechanical Engineers, Part L: Journal of Materials Design and Applications* 227 (Jan. 2013), pp. 82–88. DOI: 10.1177/1464420712451806.

[20]   Hallquist, John. *LS-DYNA THEORY MANUAL*. English. Livermore Software Technology Corporation. 680 pp.

[21]   Erhart, Tobias. *Review of Solid Element Formulations in LS-DYNA*. LS-DYNA Forum. 2011. URL: https://www.dynamore.de/de/download/papers/forum11/entwicklerforum-2011/erhart.pdf.

[22]   *LS-DYNA KEYWORD USER'S MANUAL VOLUME II Material Models*. English. Version R13. Livermore Software Technology Corporation. 1993 pp. September 27, 2021.

[23]   Shah, Qasim H and Topa, Ameen. "Modeling large deformation and failure of expanded polystyrene crushable foam using LS-DYNA". In: *Modelling and Simulation in Engineering* 2014 (2014).

[24]   Owen, Emily. *LS-DYNA Introduction to contacts*. Webinar. 2020. URL: https://www.oasys-software.com/dyna/wp-content/uploads/2020/01/Intro-to-Contacts.pdf.

[25]   Ouellet, Simon, Cronin, Duane, and Worswick, Michael. "Compressive response of polymeric foams under quasi-static, medium and high strain rate conditions". In: *Polymer Testing* 25.6 (2006), pp. 731–743. ISSN: 0142-9418. DOI: https://doi.org/10.1016/j.polymertesting.2006.05.005. URL: https://www.sciencedirect.com/science/article/pii/S0142941806000973.

Appendix - Contents

Appendix A

Experimental test figures

This Appendix shows the plots from the crown and back impact tests, for the velocities of 6.50 m/s and 7.70 m/s.
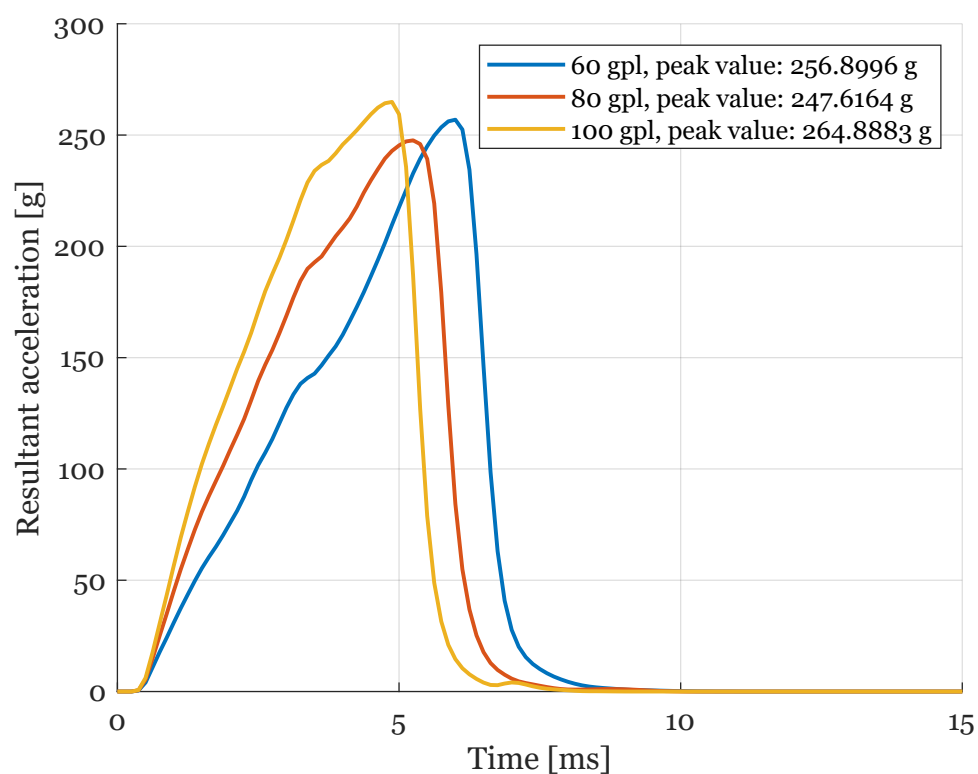
A.0.1   Crown impact
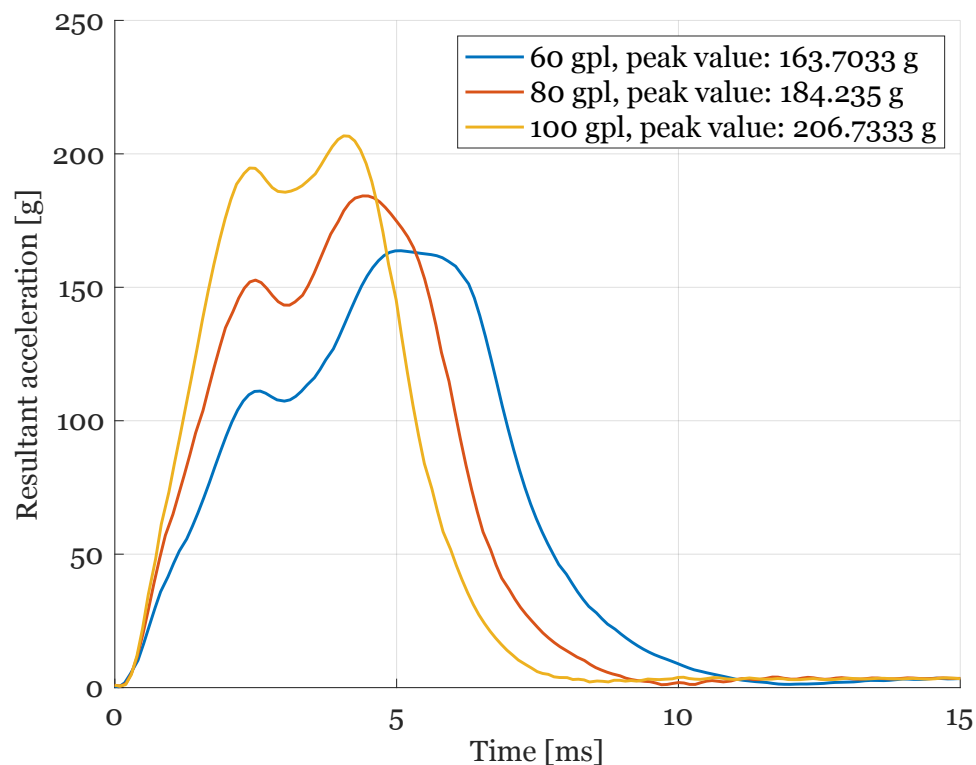
Figure A.0.1: Crown impact for EPS densities 60, 80 and 100 gpl with impact velocity 6.50 m/s.
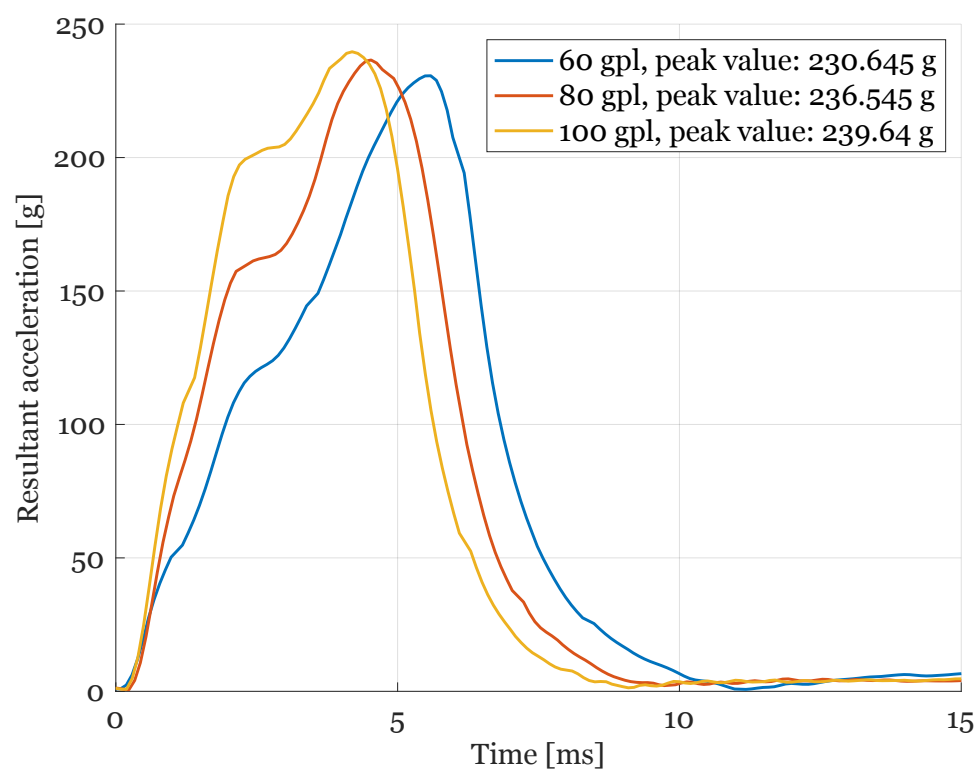
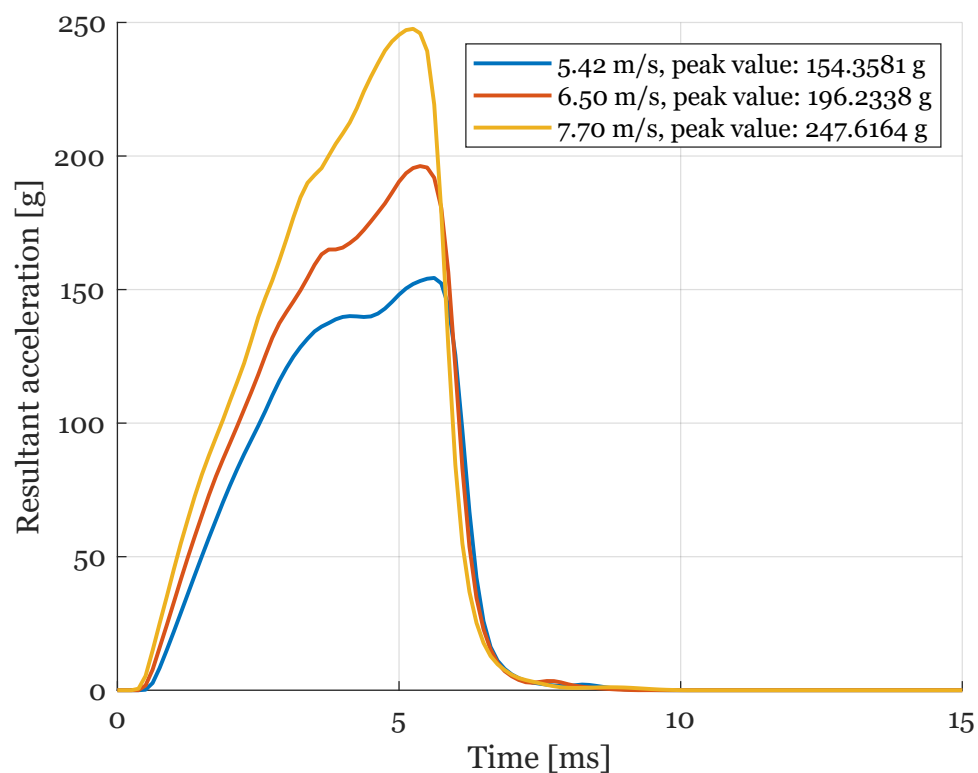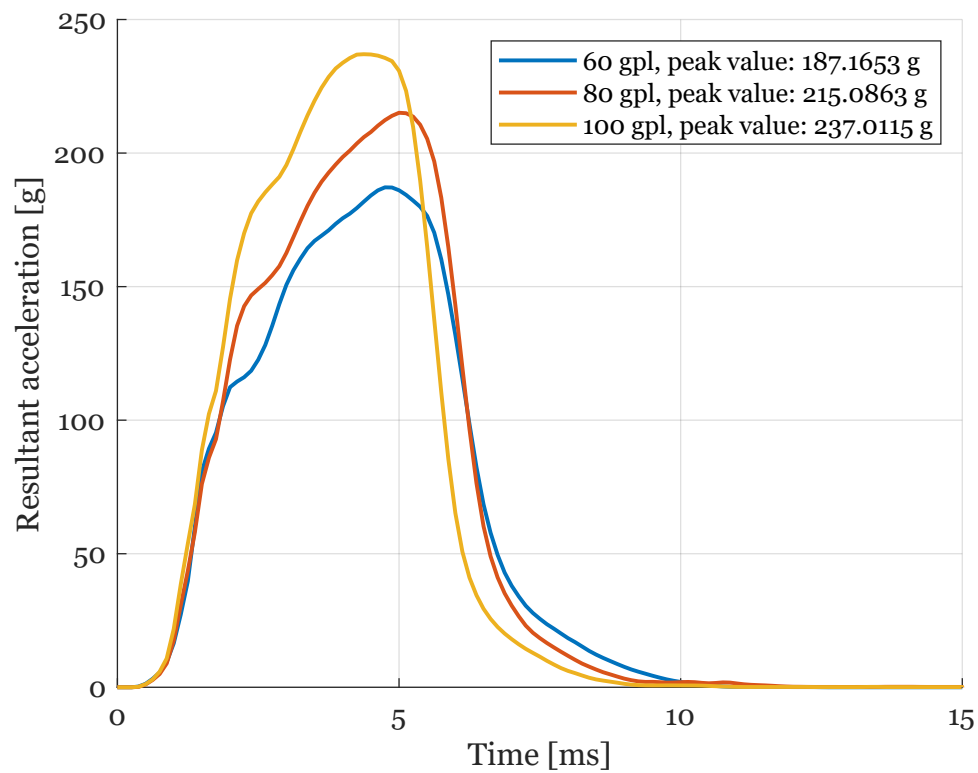Figure A.0.2: Crown impact for EPS densities 60, 80 and 100 gpl with impact velocity 7.70 m/s.

A.0.2 Back impact
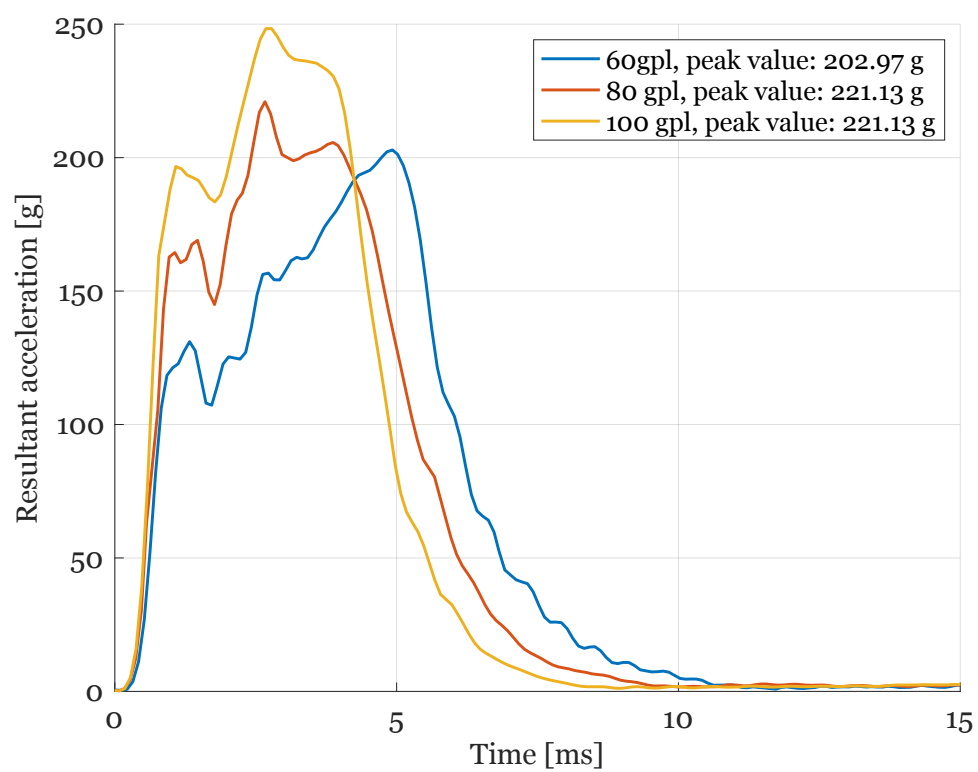
Figure A.0.3: Back impact for EPS densities 60, 80 and 100 gpl with impact velocity 7.70 m/s.

Appendix B

FE-simulation figures

The remaining acceleration plots for crown and back from the FEA are presented in this Appendix.

B.0.1   Crown impact
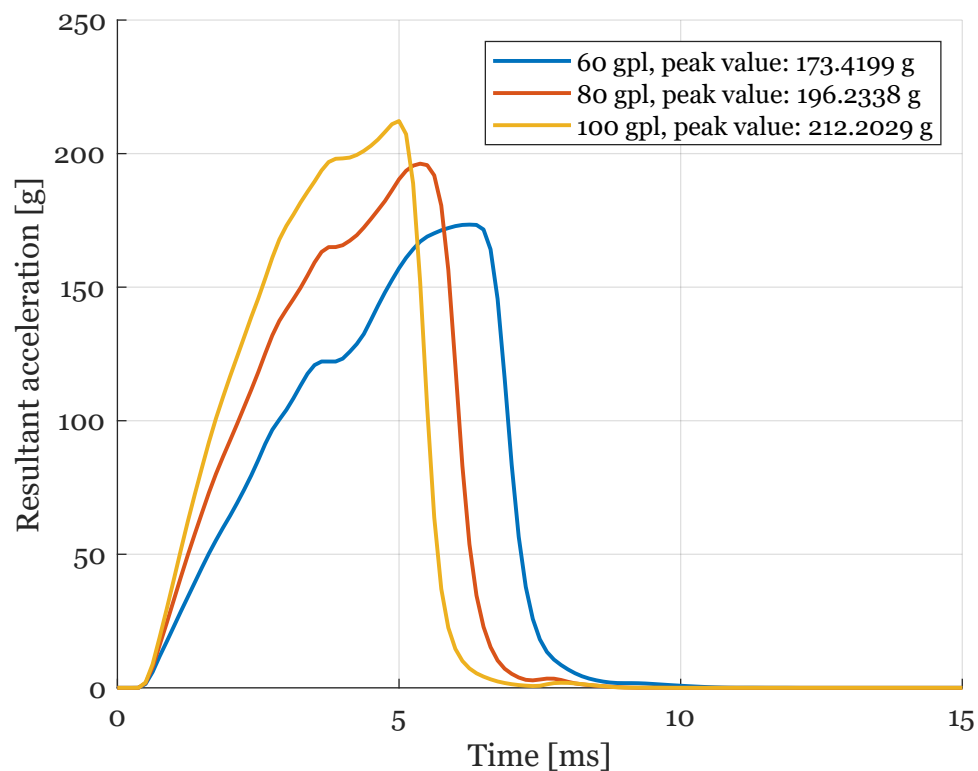
Figure B.0.1: Crown impact for EPS densities 60, 80 and 100 gpl with impact velocity 6.50 m/s.

Figure B.0.2: Crown impact for EPS densities 60, 80 and 100 gpl with impact velocity 7.70 m/s.

Figure B.0.3: Crown impact for EPS with density 80 gpl and impact velocities 5.42, 6.50 and 7.70 m/s.
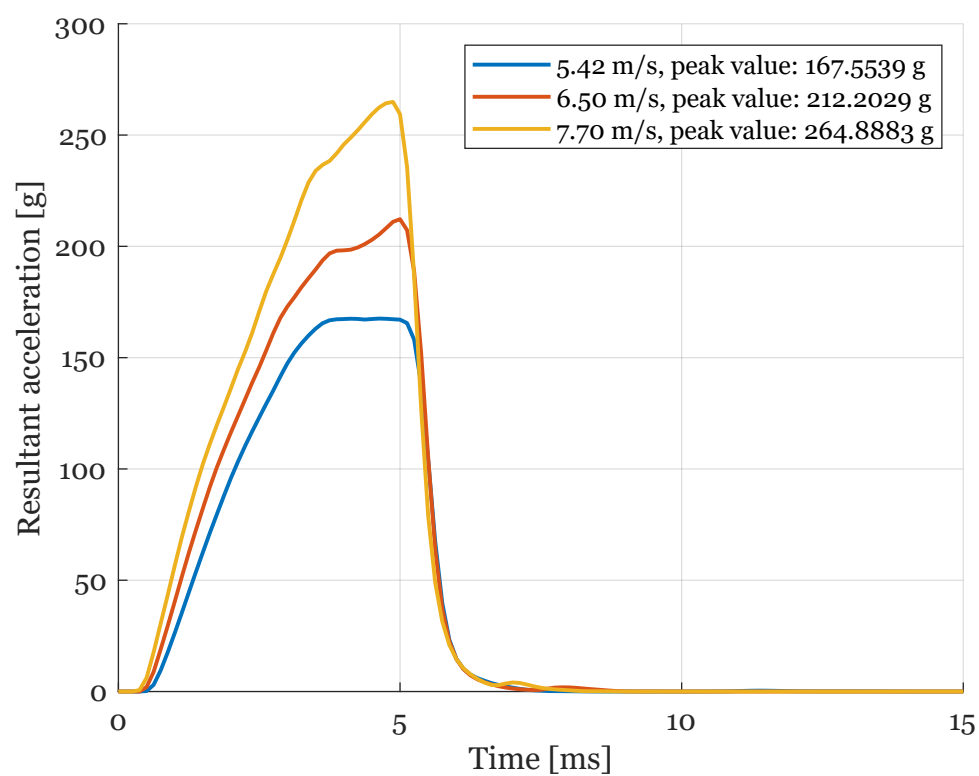
Figure B.0.4: Crown impact for EPS with density 100 gpl and impact velocities 5.42, 6.50 and 7.70 m/s.

B.0.2 Back impact

Figure B.0.5: Back impact for EPS densities 60, 80 and 100 gpl with impact velocity 7.70 m/s.
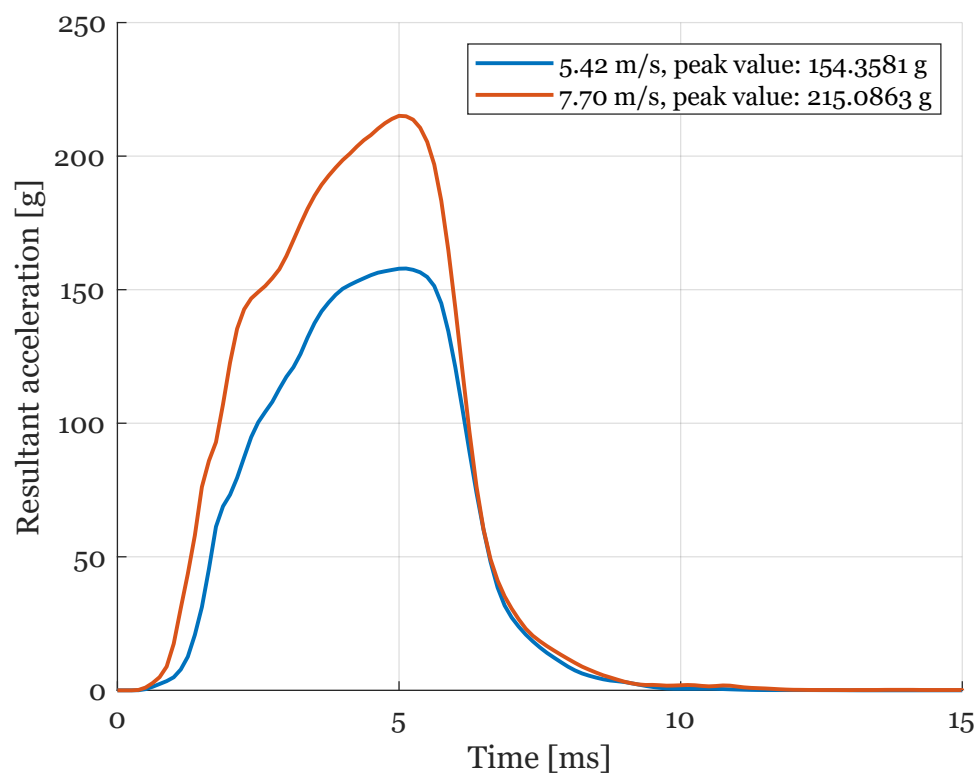
Figure B.0.6: Back impact for EPS with density 80 gpl and impact velocities 5.42 and 7.70 m/s.
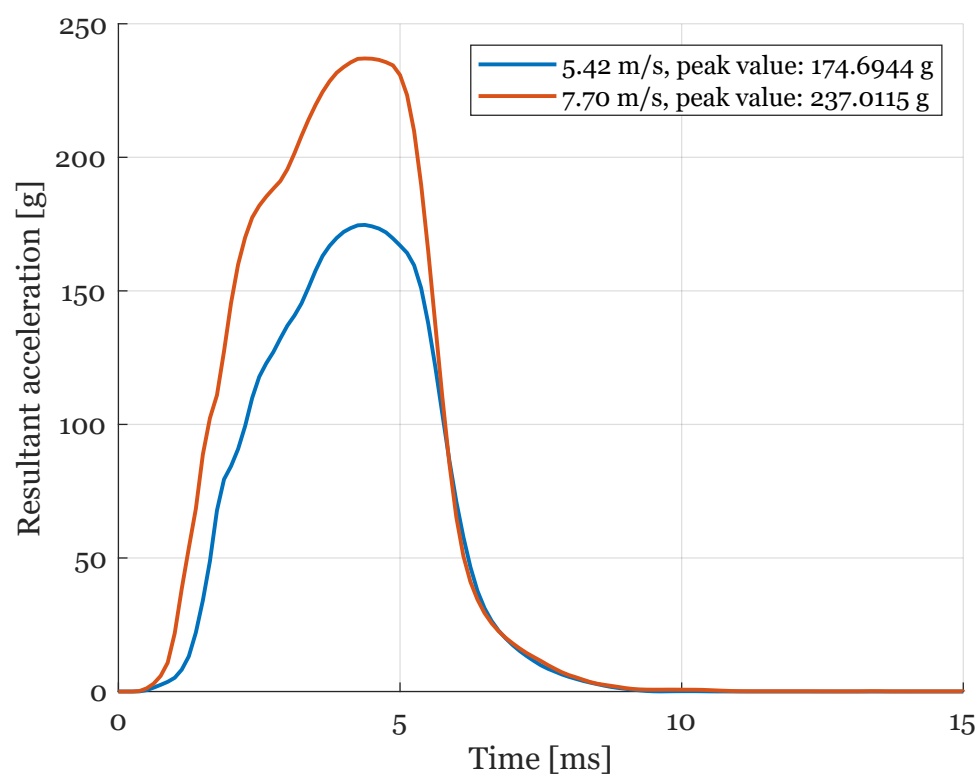
Figure B.0.7: Back impact for EPS with density 100 gpl and impact velocities 5.42 and 7.70 m/s.

Appendix C

FE-parametric study figures

In this Appendix, the plots from the EPS thickness parameter study are presented for the 80 gpl and 100 gpl densities.

C.0.1 EPS thickness
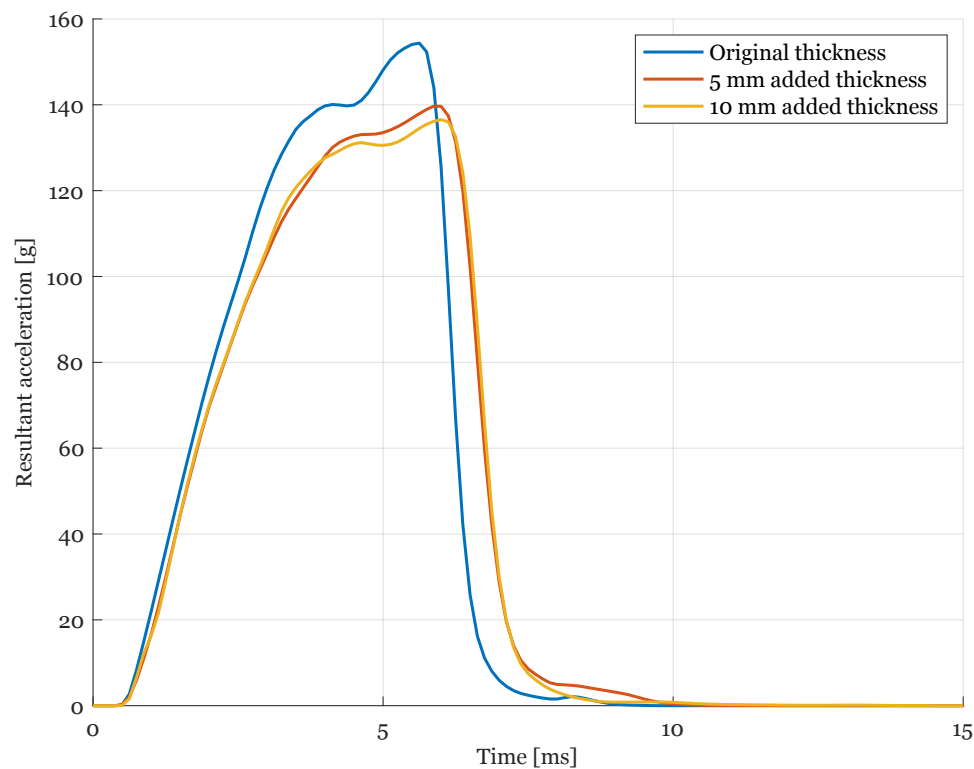
Figure C.0.1: Crown impact for EPS density 80 gpl with impact velocity 5.42 m/s.
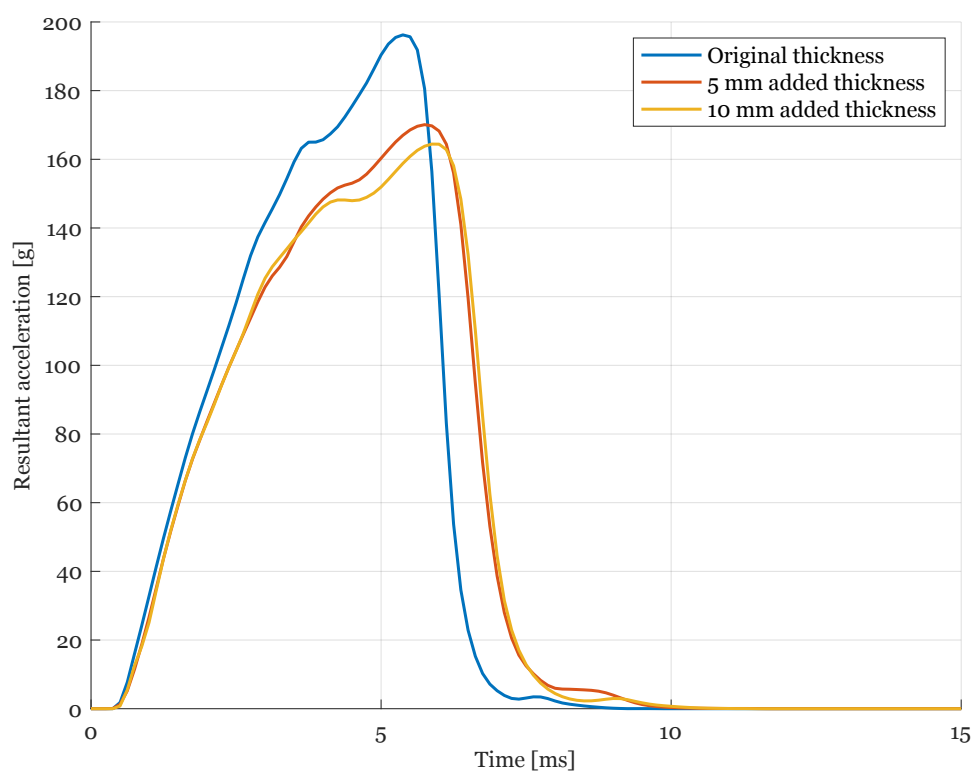
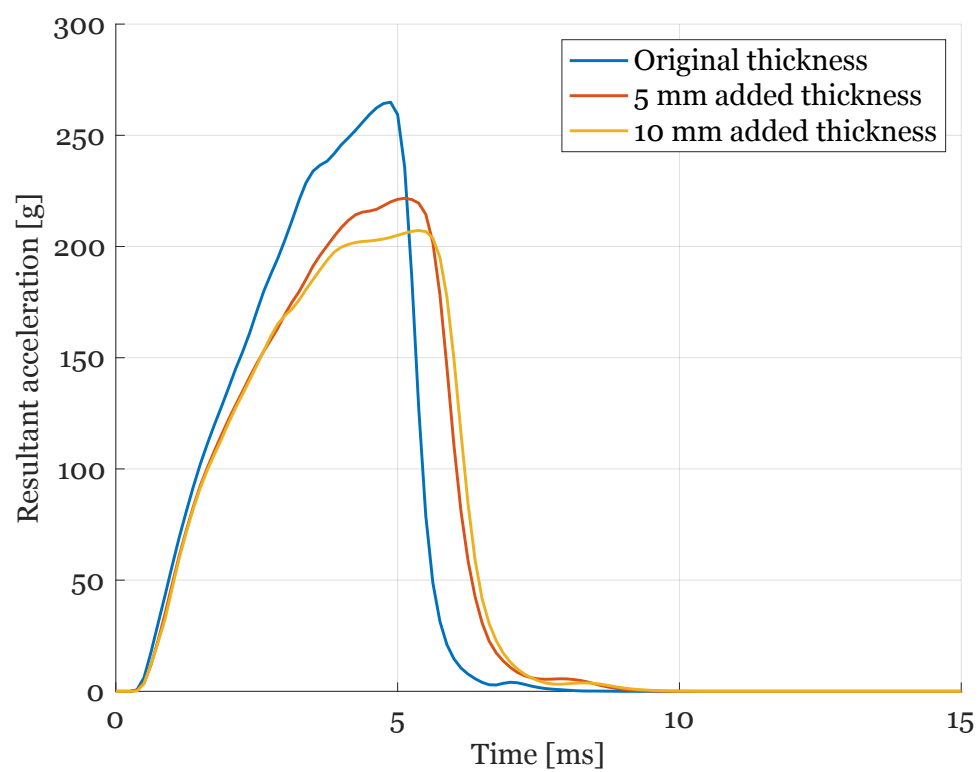Figure C.0.2: Crown impact for EPS density 80 gpl with impact velocity 6.50 m/s.
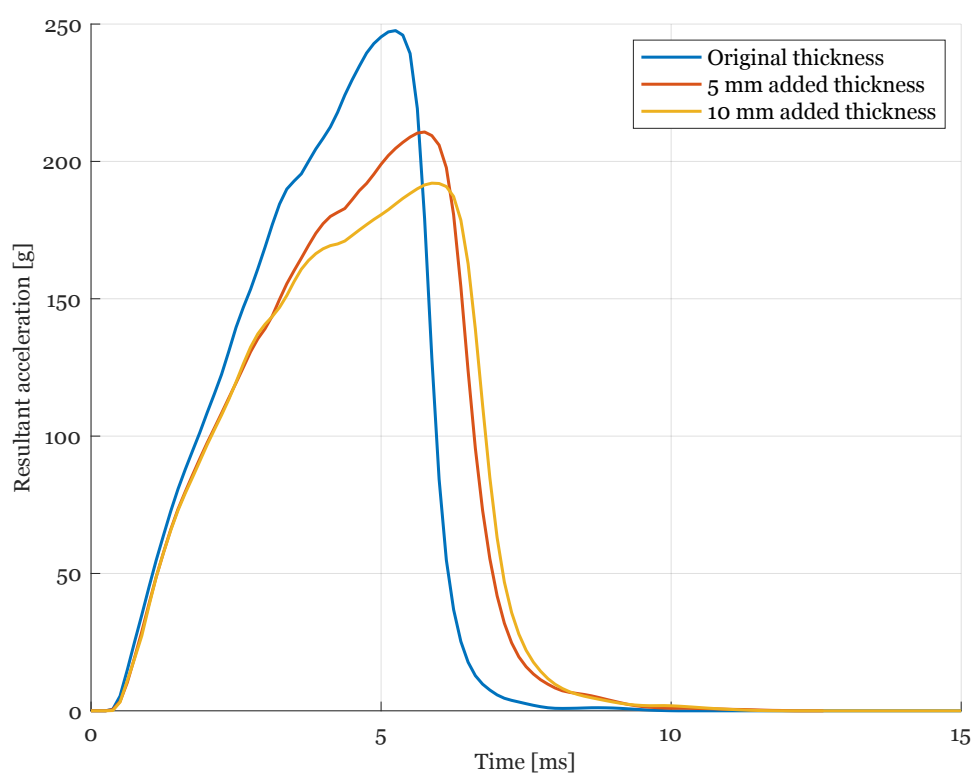
Figure C.0.3: Crown impact for EPS density 80 gpl with impact velocity 7.70 m/s.
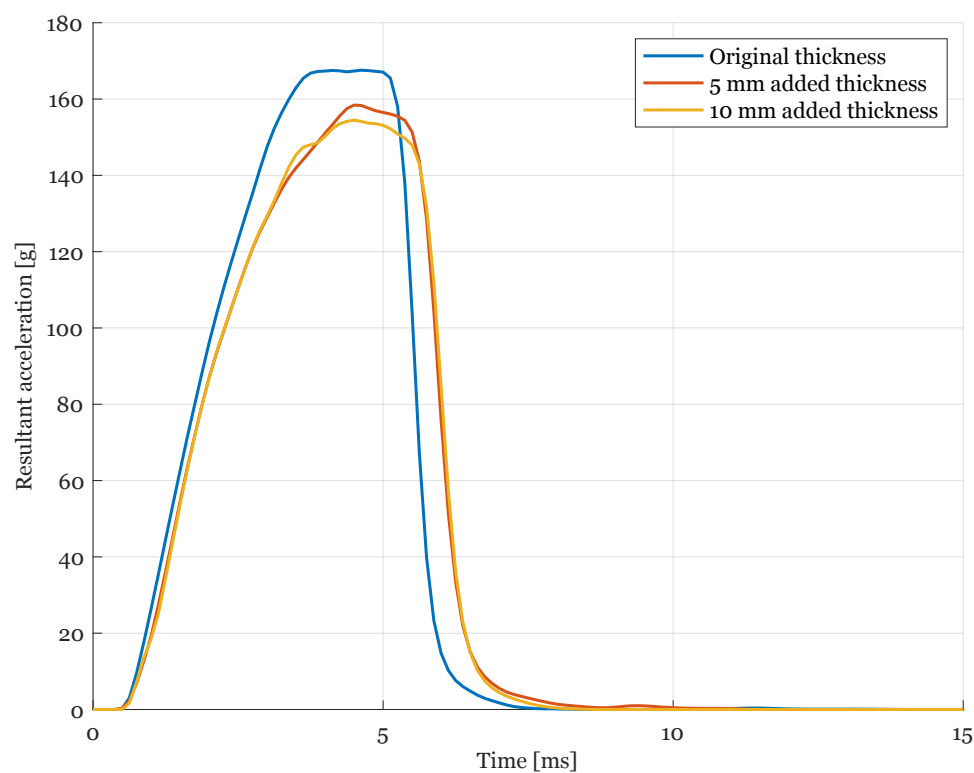
Figure C.0.4: Crown impact for EPS density 100 gpl with impact velocity 5.42 m/s.
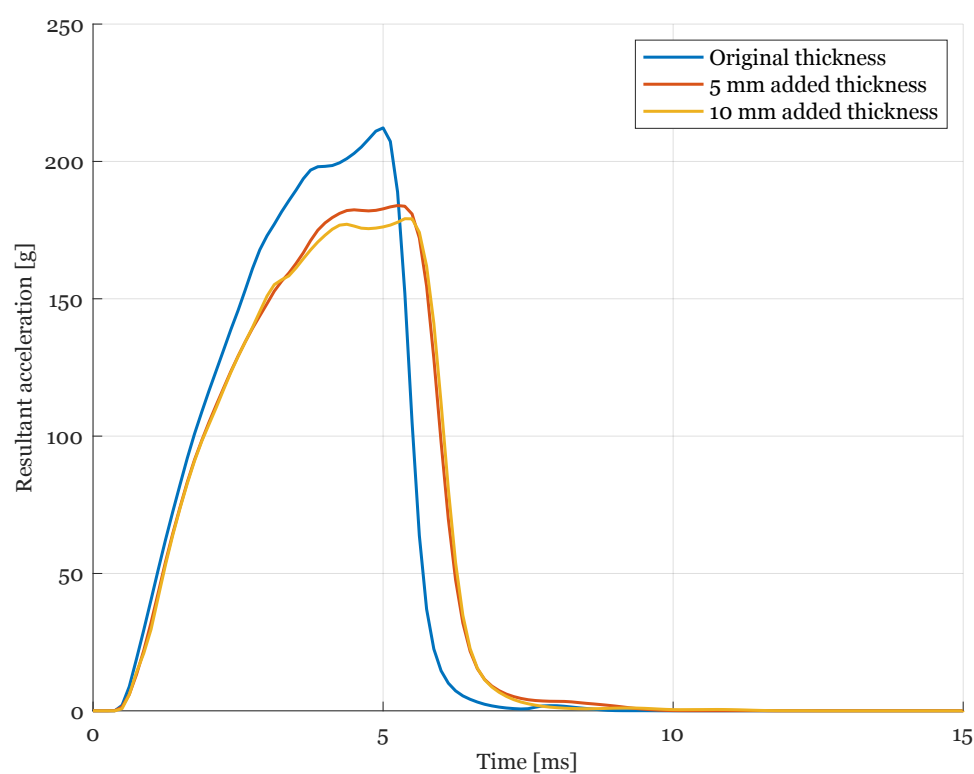
Figure C.0.5: Crown impact for EPS density 100 gpl with impact velocity 6.50 m/s.

Figure C.0.6: Crown impact for EPS density 100 gpl with impact velocity 7.70 m/s.

Appendix D

Result summary figures

This Appendix presents the remaining results from the comparison study between the linear impact test and simulation, for the 80 gpl and 100 gpl densities.

D.0.1 Crown impact
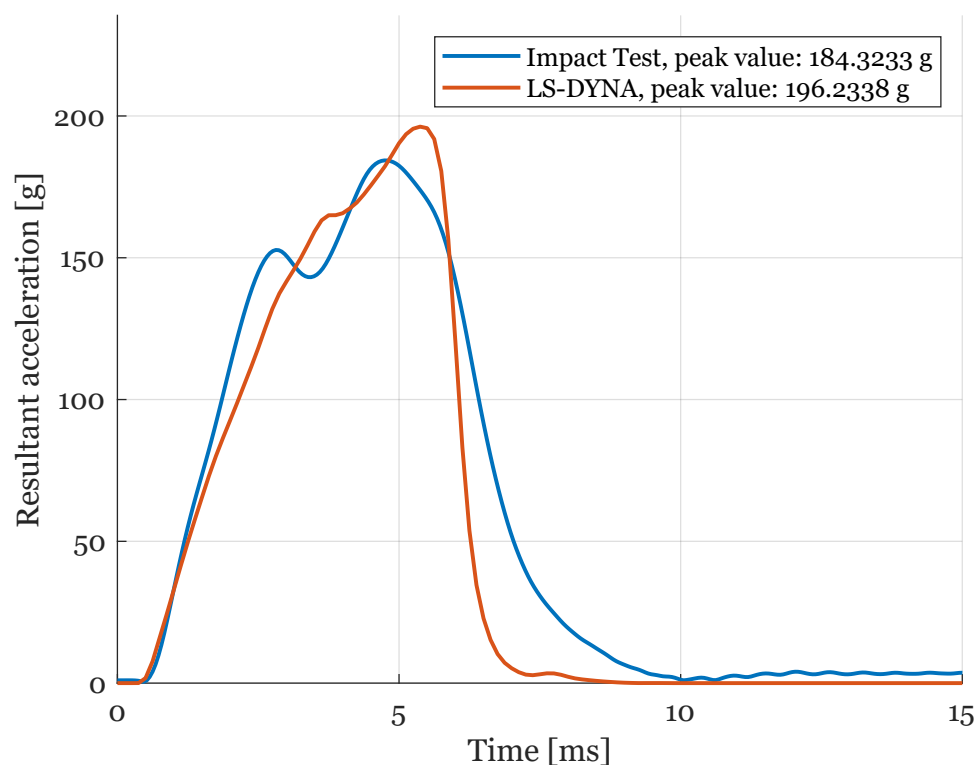
Figure D.0.1: Experimental and simulation results for crown impact with density 80 gpl and velocity 6.5 m/s.
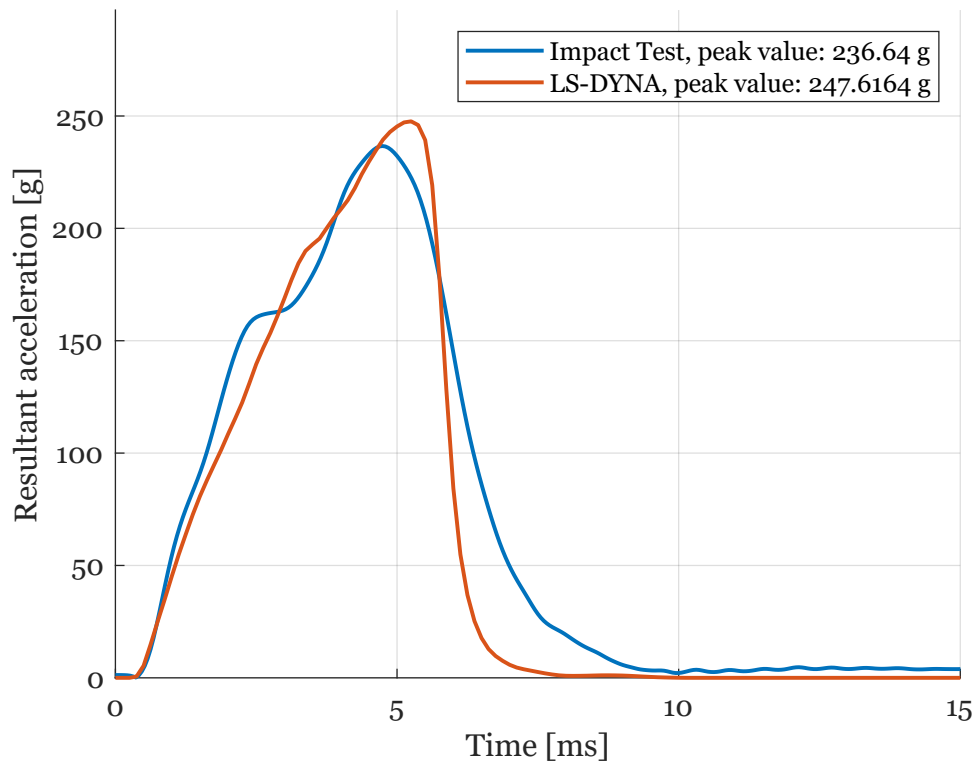
Figure D.0.2: Experimental and simulation results for crown impact with density 80 gpl and velocity 7.7 m/s.
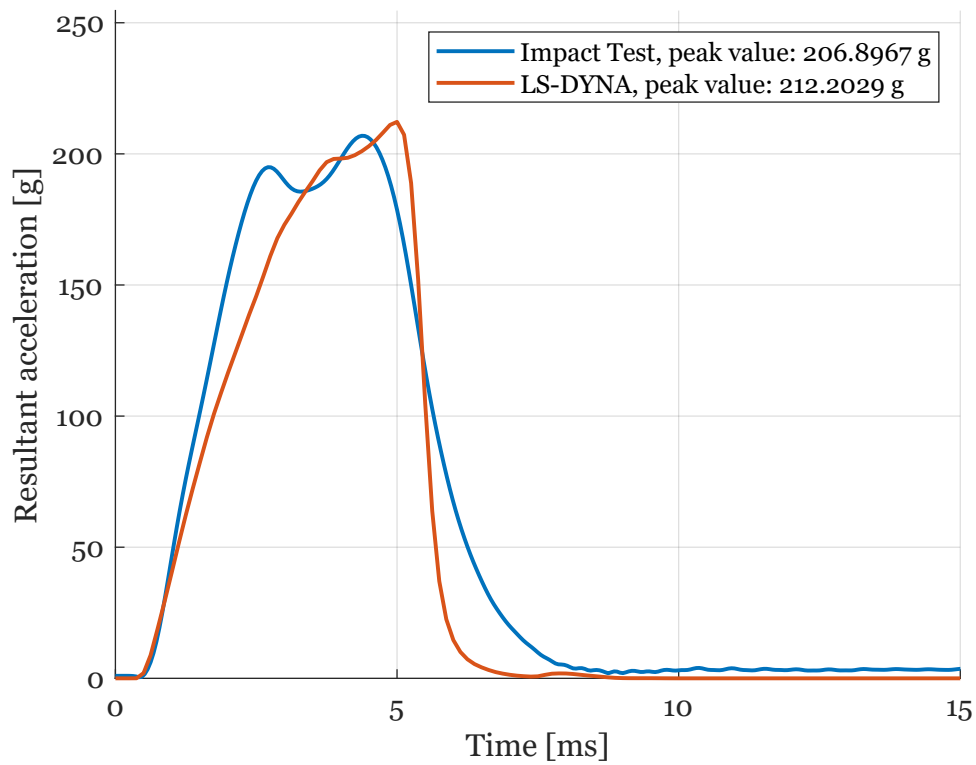

Figure D.0.3: Experimental and simulation results for crown impact with density 100 gpl and velocity 6.5 m/s.
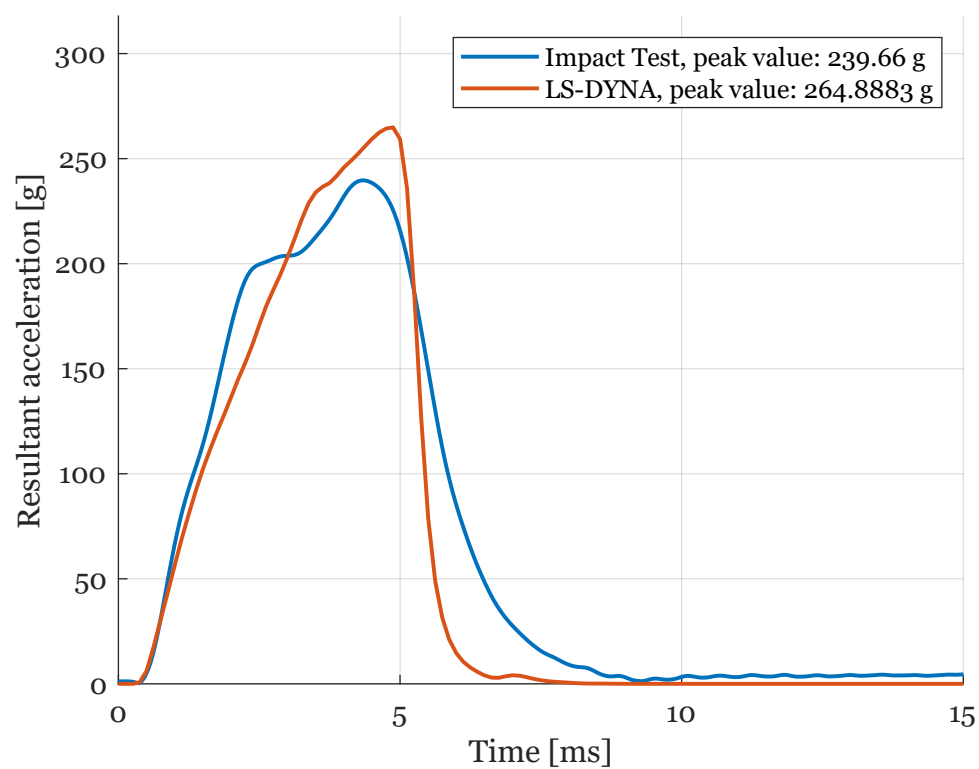
Figure D.0.4: Experimental and simulation results for crown impact with density 100 gpl and velocity 7.7 m/s.
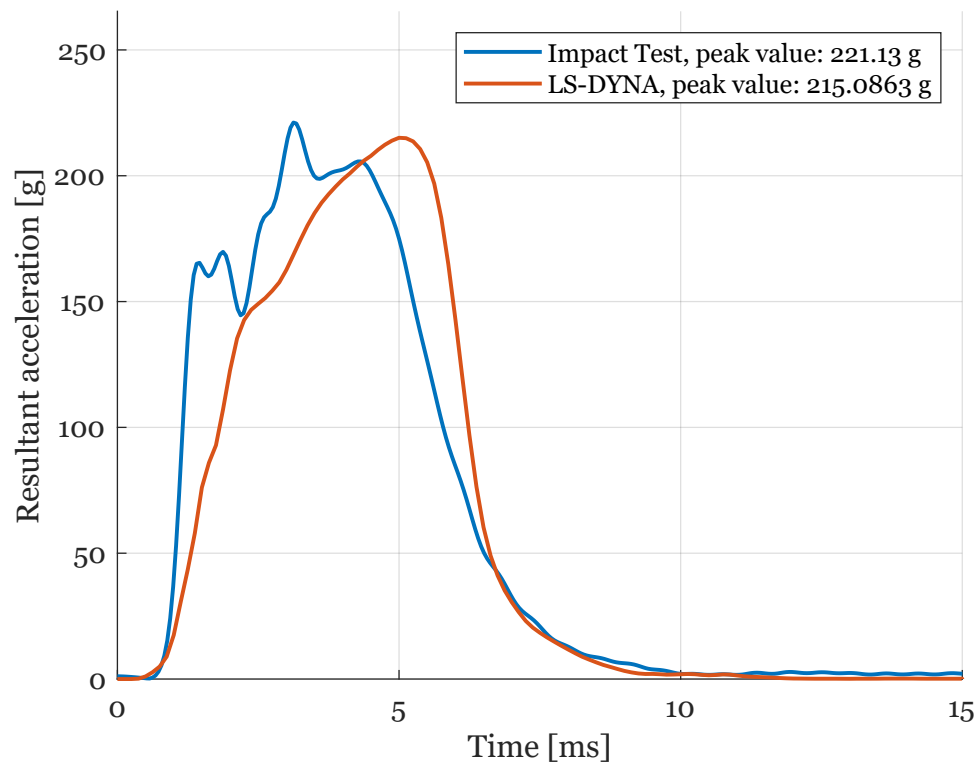
D.0.2 Back impact

Figure D.0.5: Experimental and simulation results for back impact with density 80 gpl and velocity 7.7 m/s.
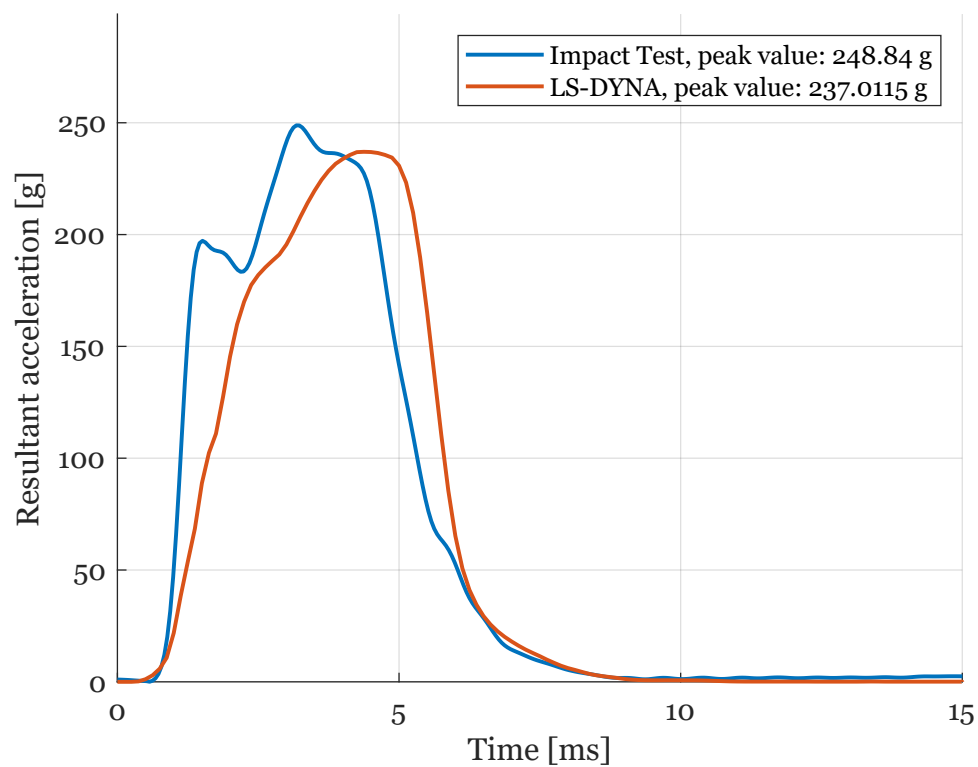
Figure D.0.6: Experimental and simulation results for back impact with density 100 gpl and velocity 7.7 m/s.